

Jagiellonian University

Faculty of Physics, Astronomy and Applied Computer Science



Gabriela Łapkiewicz

Student's number: 135030

Determining positronium lifetimes in uniform samples of aluminum, copper, nickel and quartz using modular J-PET scanner and Biograph Vision Quadra scanner

Master Thesis in Biophysics

Supervised by
dr Szymon Niedźwiecki Department of Experimental
Particle Physics and Applications

Kraków 2024

Oświadczenie autora pracy

Świadoma odpowiedzialności prawnej oświadczam, że niniejsza praca dyplomowa została napisana przeze mnie samodzielnie i nie zawiera treści uzyskanych w sposób niezgodny z obowiązującymi przepisami.

Oświadczam również, że przedstawiona praca nie była wcześniej przedmiotem procedur związanych z uzyskaniem tytułu zawodowego w wyższej uczelni.

.....
Kraków, dnia

.....
Podpis autora pracy

Oświadczenie kierującego pracą

Potwierdzam, że niniejsza praca została przygotowana pod moim kierunkiem i kwalifikuje się do przedstawienia jej w postępowaniu o nadanie tytułu zawodowego.

.....
Kraków, dnia

.....
Podpis kierującego pracą

Acknowledgements

Foremost I would like to thank Profesor Paweł Moskal, for opportunity to be part of his research group. I would like to thank Professor Axel Rominger, Professor Kuangyu Shi and Professor Ewa Stepień for the opportunity to participate in the experiments at the Inselhospital in Bern. I am deeply grateful to my supervisor Doctor Szymon Niedźwiecki for his guidance during my time at the Jagiellonian University, the time he dedicated and the knowledge he shared with me.

I would also like to thank Doctor William Steinberger for his contribution and Doctor Kamil Dulski for his comments on my analysis.

I wish to thank my friends: Ola, Weronika and Arseny, for moral support, motivation and the ambience during my writing of this thesis. Dziękuję moim Rodzicom za umożliwienie mi kształcenia się i wsparcie podczas nauki i pisania pracy.

Research presented in this thesis was supported by the National Science Centre through grants 2021/42/A/ST2/00423 (lead by Prof. Paweł Moskal), 2022/47/I/NZ7/03112 (lead by Prof. Ewa Stepień and Prof. Kuangyu Shi).

Abstract

Positronium imaging is a tool that could raise the specificity of medical imaging. A part of the development of the positronium imaging technique is establishing the method for the assessment of detector imaging precision and comparison of the results obtained between various scanners.

This thesis presents the methods and results of positronium imaging of 4 materials performed with modular J-PET and Biograph Vision Quadra PET/CT scanners and compares them with Positronium Annihilation Lifetime Spectroscopy studies of the same samples. The compared materials were disks of quartz glass and 3 metals of high purity: aluminum, nickel and copper. The metal samples spectra are expected to be characterised by short-living components that correspond to positrons directly annihilating in the metal lattice. The mean lifetime of positron in such samples are dependent on the lattice parameters but may be influenced by the lattice defects. The quartz glass is an amorphous substance that is characterised by the ortho-positronium mean lifetime in range representative for biological tissues.

A hypothesis was formulated that that it is possible to obtain the positronium mean lifetime spectra with three detection systems presented in this thesis and analysis of the spectra will yield similar results: the quartz glass will stand out by longer component of ortho-positronium lifetime in comparison with metal samples.

To test the stated hypothesis, the author had performed measurements on PALS system and modular J-PET scanner, preselected the data using dedicated software and analysed the spectra with PALS Avalanche software. Author had also performed analysis of the spectra obtained with Biograph Vision Quadra.

This work have shown that the applied method of measurement and analysis is applicable for each of the presented setup. The percentage difference between mean lifetime values obtained with PALS and Biograph Vision Quadra scanner does not exceed 7%. The percentage difference between mean lifetime values obtained with PALS and modular J-PET scanner does not exceed 30%. The stated hypothesis was proven that in all measurement setups it is possible to differentiate between quartz glass and metal, based on the mean lifetime of ortho-positronium and positron mean lifetime components.

Streszczenie

Obrazowanie pozytonium jest narzędziem, które może podnieść swoistość obrazowania medycznego. W ramach rozwoju techniki obrazowania pozytonium ważne jest opracowanie metody określenia precyzji obrazowania i porównania rezultatów otrzymanych za pomocą różnych skanerów.

Ta praca prezentuje metody i rezultaty obrazowania pozytonium wykonanego na 4 materiałach za pomocą modularnego skanera J-PET i skanera PET/CT Biograph Vision Quadra oraz porównuje je z wynikami pomiarów wykonanych za pomocą metody Spektroskopii Czasu Życia Pozytonium. Porównywanymi materiałami były dyski wykonane ze szkła kwarcowego oraz trzech metali o wysokiej czystości: aluminium, niklu i miedzi. Widma czasu życia dla próbek metali charakteryzują się krótkożyciowymi składowymi, które odpowiadają bezpośredniej anihilacji pozytonów w sieci krystalicznej metali. Średni czas życia pozytonu w takiej próbce zależny jest od właściwości sieci, ale wpływać na niego może także obecność defektów. Szkło kwarcowe jest substancją amorficzną, która charakteryzuje się średnim czasem życia reprezentatywnym dla tkanek biologicznych.

Sformuowana została hipoteza badawcza, że możliwym jest otrzymanie widma średniego czasu życia pozytonium za pomocą trzech układów zaprezentowanych w tej pracy, oraz że analiza widm pozwoli na uzyskanie zbliżonych wyników: widmo czasu życia dla kwarcu będzie wyróżniać się dłuższym czasem życia w porównaniu z próbkami metali.

Aby sprawdzić hipotezę badawczą autorka tej pracy wykonała pomiary za pomocą układu PALS i modularnego skanera J-PET, a także preselekcję danych z wykorzystaniem dedykowanego oprogramowania i zanalizowała widma przy użyciu programu PALS Avalanche. Autorka dokonała także analizy widm otrzymanych z pomiarów skanerem Biograph Vision Quadra.

Praca ukazała, że zastosowane metody pomiarów i analizy widm czasów życia są stosowalne dla każdego z zaprezentowanych układów. Różnice procentowe pomiędzy średnimi czasami życia otrzymanymi z pomiarów skanerem Biograph Vision Quadra i spektroskopem PAL nie przekraczają 7%. Różnice procentowe między średnimi czasami życia otrzymanymi za pomocą spektroskopu PAL i modularnego skanera J-PET nie przekraczają 30 %. Analiza wyników potwierdziła hipotezę badawczą wykazując, że rozróżnienie między próbkami szkła kwarcowego i metalem w oparciu o średni czas życia ortho-pozytonium w kwarcu i średni czas życia pozytonów w metalu jest możliwe we wszystkich przedstawionych układach pomiarowych.

Contents

1	Introduction	8
2	Thesis goal	10
3	Positronium	12
3.1	Positronium bound state	12
3.2	Positronium decay mechanisms in matter	13
3.2.1	Pick-off models	14
3.3	Positronium Annihilation Lifetime Spectroscopy	15
3.4	Positron annihilation in metals	16
3.5	Positronium imaging in medical diagnostics	18
3.5.1	Positronium in cancer	18
3.5.2	Other applications in medicine	20
3.6	Positronium imaging	21
3.7	Radionuclides for positronium imaging	22
3.8	Positron range	24
3.9	Exemplary positronium detection systems	25
4	Experimental methods	28
4.1	Sources	29
4.2	Samples	31
4.3	Measurements with Positronium Annihilation Lifetime Spectroscopy	32
4.3.1	Experimental setup	32
4.3.2	Sample preparation	33
4.3.3	Measurements	35
4.3.4	Signal analysis	36
4.3.5	Data preselection	37
4.4	Measurements with J-PET scanner	38
4.4.1	Experimental setup	38
4.4.2	Measurements	39
4.4.3	Data preselection	41
4.5	Measurements with Biograph Vision Quadra	44
4.5.1	Scanner characteristics	44
4.5.2	Measurements methodology	44
4.5.3	Data preselection	45
5	Analysis	46
5.1	PALS Avalanche	46
5.2	Fitting configuration	46

5.3	Determining the parameters for kapton and parafilm	48
5.4	Analysis of data from PALS	52
5.5	Analysis of data from modular J-PET scanner	53
5.6	Analysis of data from Biograph Vision Quadra	55
6	Results	58
6.1	PALS	58
6.2	Modular J-PET	58
6.3	Biograph Vision Quadra	59
6.4	Comparison	59
6.4.1	Time resolution of detection setups	59
6.4.2	Mean lifetimes	61
6.4.3	Goodness of the fit	62
6.4.4	Intensities	63
6.4.5	Total number of counts	64
6.4.6	Width of the bins	64
7	Summary and perspectives	65
8	Appendix A - fitted spectra	73
8.1	PALS measurements spectra	73
8.2	J-PET measurements spectra	78
8.3	Biograph Vision Quadra measurements spectra	81

1. Introduction

Positronium is a short-living bound state of positron and electron, with the rest energy of 1022 keV. It occurs in two spin states: triplet ortho-positronium and singlet para-positronium. The ortho-positronium mean lifetime in vacuum is three magnitudes longer than para-positronium mean lifetime and can be significantly shortened in molecular media due to interactions with electrons. About 40% of positrons that are emitted during the medical PET imaging create positronium in the patient's body [1]. The positronium lifetime depends on structure and molecular composition of the surrounding matter. This relationship points to a potential of the positronium as a biomarker, which could raise the specificity of the PET imaging [2, 3].

The positronium imaging technique has been proposed at the Jagiellonian University by Professor Paweł Moskal and is currently being developed as a tool for raising the specificity of PET imaging [4].

Additionally to standard PET imaging, which allows for imaging the distribution of radiopharmaceutical in patient body, the positronium imaging technique focuses on analysing the positronium lifetime spectra extracted for chosen voxels of activity or regions of interest. The analysis of such data can yield informations about internal structure of the tissue and its molecular composition. It has been shown that positronium annihilation rate is dependent on the tissue type and may change due to progression of the disease [2, 4–8]. The idea of applying positronium lifetime spectroscopy for biological studies has been a recent development and there is a necessity for further studies that examine the differences in positronium lifetime values between the healthy and diseased tissues as well as the factors that may impact the spectra shape before the positronium imaging technique can be used in clinical settings.

The progression of medical diagnostics also involves advancement in the medical equipment. Alternative to common PET imaging, which requires registration of two annihilation photons, positronium imaging requires registration of 3 photons: one deexcitation and two annihilation gamma quanta. Therefore a detector eligible for performing this technique must be adjusted for multi-photon imaging and image reconstruction [4, 9, 10]. The positronium imaging feasibility had been successfully simulated and later empirically proven with the J-PET detector [11, 12]. The studies of cardiac myxoma and adipose tissue with the J-PET scanner had shown that there are significant differences in lifetime spectra between healthy and diseased tissues [13, 14]. Recently, a first in vivo image of human brain had been obtained with the modular J-PET scanner [15].

Before applying the technique in clinical diagnostics, the detectors have to be properly assessed for their imaging precision. For this purpose it is imperative to design a phantom that would allow for qualitative assessment of scanners. A positronium imaging phantom had been previously proposed by the author, that utilised mixtures of XAD4 aerogel and water, which allowed for controlling the mean ortho-positronium lifetime component, but was susceptible to impact of environmental conditions during the preparation [16, 17]. The improved method of phantom preparation would allow for better repeatability of the measurement procedure and draw focus away from the process of phantom preparation. Thus, for the initial approach solid samples were used instead of a phantom in order to simplify the experimental task.

The aim of this thesis is to present the comparison of the values of the components of the positronium lifetime spectra obtained with three different detection systems. The

comparison presented here is between the PALS system, which uses a well established method for positronium lifetime estimation and two PET detectors eligible for positronium imaging [18–21]. The first one is the Modular J-PET scanner that has been devised by the J-PET collaboration under Professor Paweł Moskal at the Jagiellonian University and consists of plastic scintillators [22, 23]. The second scanner presented in this thesis is the Biograph Vision Quadra PET/CT scanner produced by Siemens Healthineers currently used in a clinical setting for PET imaging [24] and has been recently shown capable of performing positronium lifetime imaging [10].

Chapter 2 contains description of the goal of this thesis.

Chapter 3 of this thesis is based on literature studies performed by the author. This chapter contains theoretical introduction to the positronium bound state, the basic models describing the positronium formation and interactions with matter and the Positronium Annihilation Lifetime Spectroscopy. The later part of this chapter introduces the concept of positronium imaging and presents state of the knowledge about the positronium lifetime in various biological systems. The chapter ends with an overview of the characteristics of an exemplary systems for positronium imaging.

Chapter 4 presents the the description of the samples, sources and experimental setups. The detectors are described along the conducted measurements and preselection of the data with the dedicated softwares for PALS and Modular J-PET.

Chapter 5 describes the analysis of the lifetime spectra done with the PALS Avalanche software. In this chapter is presented the fitting procedure for establishing the values of components for the layers encapsulating the source is presented in this chapter.

Chapter 6 presents comparison of the results for each sample and detector and later discusses the factors influencing the measurements precision.

The last chapter summarises obtained results and presents perspectives of their application in creating a method for evaluating the scanner precision in view of development of the positronium imaging technique.

An appendix can be found at the end of this thesis, in which all the fitted spectra are presented along with tables of final results for each fitted spectra.

2. Thesis goal

The aim of this thesis is to compare the results of positronium imaging performed with two PET scanners and the mean lifetime spectra obtained with Positronium Annihilation Lifetime Spectroscopy present at Jagiellonian University. The two PET scanners are the modular Jagiellonian-PET at Jagiellonian University in Kraków and the Biograph Vision Quadra PET/CT scanner produced by Siemens Healthineers present at the Inselhospital in Bern, Switzerland.

The detectors used in this study differ in both hardware and software. The PALS system is built from two BaF_2 scintillators connected to photomultipliers and registers annihilation and deexcitation gamma quanta within the set coincidence window [8]. The modular J-PET scanner is built from plastic scintillators organised axially and Biograph Vision Quadra PET/CT scanner is composed of crystal scintillators organised radially [15, 23, 25]. The PET scanners calibrated for positronium imaging can be used to obtain the lifetime spectra for chosen voxel or region of interest additionally to the distribution of the points of emission [26, 27].

The subject of this study are the disks composed of quartz glass and various metals: aluminum, copper and nickel. The quartz glass is an amorphous substance with mean o-Ps lifetime around 1.5 ns [10, 28, 29], similar to the lifetime values that can be found in biological material [5, 8, 21, 30]. The lifetime spectra of metal samples is expected to be composed of shorter-living components. Metals are characterised by direct positron annihilation component in metal lattice [31].

The study presented here is a step in development of a positronium imaging phantom. The author of this thesis had previously proposed a phantom for positronium imaging precision quantitative assessment as a subject of the Bachelor thesis [17]. Such phantom consisted of six volumes of high activity immersed in low activity background. Each of the sphere contained mixtures of XAD and water of various mass percentage, which were characterised by different lifetimes of o-Ps. The study has shown that there is dependency of mean ortho-positronium lifetime on concentration of XAD in water and that it can be used for adjusting the lifetime of positronium for the purpose of assessment of scanner precision of determining the positronium lifetime. Unfortunately it is difficult to precisely control the positronium lifetimes in this manner due to high dependency on environmental conditions during its preparation. To correctly evaluate the differences in results from multiple systems it is required to design a repeatable method of positronium imaging quality assessment.

Alternatively, a positronium imaging phantom can be composed of materials with established, invariable lifetime values that represent the range of lifetimes encountered in medical imaging. Additionally, it is important to see if it is possible to discern between lifetimes with smaller (tens of picoseconds) and bigger (hundreds of picoseconds) range of differences. This can be achieved by employing samples of various metals that are characterised by certain range of differences in mean lifetime value and a quartz glass, which compared with metal samples is characterised by one magnitude greater o-Ps lifetime than the mean lifetimes of positrons observed in metals. This type of phantom, that would consist of metals and quartz glass, would allow for better repeatability of the measurement procedure and draw focus away from the process of phantom preparation. A proposition of such phantom is depicted in scheme in Figure 2.1.

The possibility to control the lifetime of positronium was previously proven by the

author with measurements on PALS system. Author hypothesises that it is also possible to obtain the lifetime spectra with chosen PET scanners and the presented methods for analysis of the spectra will yield similar results between the measurement systems.

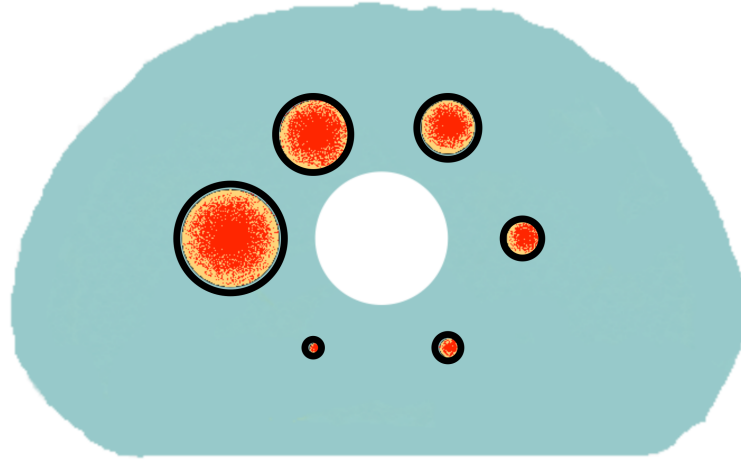


Figure 2.1: The proposition of the phantom for positronium imaging method precision assessment. The phantom is constituted of 6 spheres of high activity (red circles) in lower activity background (marked by blue colour). The spheres of high activity are surrounded with metal or quartz encasement characterised by its specific mean lifetime of positrons and positronium.

3. Positronium

3.1 Positronium bound state

Positronium, presented schematically in Figure 3.1, is a meta-stable exotic atom comprised of electron and its anti-particle positron circling around their common center of mass. Both positron and electron share a mass of $511keV/c^2$ and spin $1/2$. What differentiates them is their charge: an electron is a negatively charged particle, and a positron has a positive charge [32]. Positronium appears in two states: ortho-positronium and para-positronium distinguished by the total spin state. Para-positronium is characterised by total spin (S) equal to zero and ortho-positronium total spin is equal to one. The wave-functions presented below describe the para- $\psi_{S=0,m=0}$ and ortho-positronium $\psi_{S=1,m=1}$, $\psi_{S=1,m=0}$, $\psi_{S=1,m=-1}$ combinations:

$$\begin{aligned}
 \psi_{S=0,m=0} &= \frac{1}{\sqrt{2}}(\phi_+(\uparrow)\phi_-(\downarrow) - \phi_+(\downarrow)\phi_-(\uparrow)) \\
 \psi_{S=1,m=1} &= (\phi_+(\uparrow)\phi_-(\uparrow)) \\
 \psi_{S=1,m=0} &= \frac{1}{\sqrt{2}}(\phi_+(\uparrow)\phi_+(\downarrow) - \phi_+(\downarrow)\phi_-(\uparrow)) \\
 \psi_{S=1,m=-1} &= (\phi_+(\downarrow)\phi_-(\downarrow))
 \end{aligned}
 \tag{3.1}$$

The spin statistics for para and ortho-positronium are as 1:3, pointing to three times higher probability of ortho-positronium formation [1].

Ortho-positronium mean decay time in vacuum was estimated to 142 ns and it annihilates into three or more odd number of gamma quanta with accordance to law of conservation of energy and momentum [1, 33]. Para-positronium mean decay time is 125 ps and it annihilates into two (or more even number of) gamma quanta near the angle of 180° [1, 34, 35]. Each of the two photons carry energy of 511 keV, which is equal to the rest energy of either an electron or a positron. However, in matter ortho-positronium will most likely annihilate faster due to pick off process or ortho-para conversion [1, 36, 37].

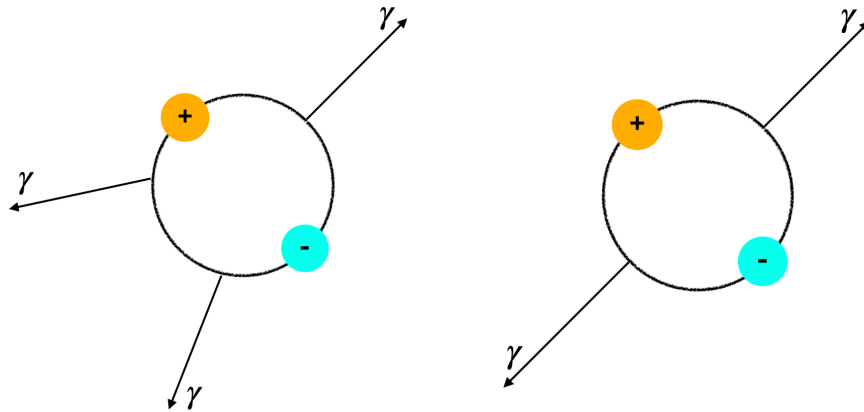


Figure 3.1: The orange circle denotes positron and the blue circle denotes electron. *Left:* Schematic depiction of ortho-positronium decaying into three gamma quanta with net energy 1022 keV. *Right:* Schematic depiction of para-positronium decaying into two gamma quanta, each with energy of 511 keV.

Right after emission, the beta particle has higher energy than it will have when it forms positronium. After its injection into matter it loses its kinetic energy by the means of ionising the surrounding molecules along its track. This process is called thermalisation. At the end of its path, when it has reached the optimal value of energy, called Ore gap, it can combine with one of the electrons that are knocked out through ionisation from a molecule. Ore's model was the first to describe the energies in which the formation of the positronium is likely:

$$E_{exc} \geq T \geq E_i - E_{Ps}, \quad (3.2)$$

Where E_{exc} is the lowest excitation energy of the molecule, T is the energy value in which formation of positronium is likely, E_i is the ionisation potential of the molecule and E_{Ps} is the binding energy of positronium in vacuum [33].

The processes that can be described by Ore model are dominant in the low-density simple atomic gases. However in condensed media the positronium binding energy decreases due to interactions with densely packed molecules. Hence the width of the Ore gap is reduced and may even disappear rendering this model of positronium formation unlikely in dense medium [38].

The models that describe the positronium formation in molecular media are spur and blob model. According to those models the positronium formation occurs when a thermalised positron combines with one of the electrons produced by ionisation of the medium at the end of the positron track. The difference between those models is in the calculations of probability of positronium formation and the details of terminal part of positron track: in spur model at the end of the track only a couple of ion-electron pairs arise whereas according to blob model the terminal part of the positron track is a bigger sphere that contains about 30 ion-electron pairs [39].

3.2 Positronium decay mechanisms in matter

After positronium is formed its lifetime depends on properties of its surroundings. In matter ortho-positronium lifetime is shortened significantly and depends strongly on the structure and composition, such as sizes of free volumes and their concentration, as well as presence of paramagnetic molecules and ions [38].

The possible decay mechanisms of positron and positronium in intramolecular spaces are:

- direct annihilation of positron with electron,

and in case of positronium formation:

- annihilation due to pick-off process,
- self-annihilation of para-positronium,
- annihilation after ortho-para conversion,
- self-annihilation of ortho-positronium [37, 40].

The most common process is the direct annihilation of positron and electron. As a result of their annihilation two gamma quanta are emitted into opposite directions with energies of 511 keV.

The pick-off process, depicted schematically in Figure 3.2, occurs when, after the formation of positronium, the positron annihilates directly with the electron from the surrounding matter, resulting in emission of two gamma quanta. The pick-off process probability is

inversely proportional to the size of the electron free voids, in a relationship described by Tao-Eldrup model [36, 41]. Depending on the molecular composure and structure of the matter, the lifetime of positronium can be impacted by the arrangement of the molecules.

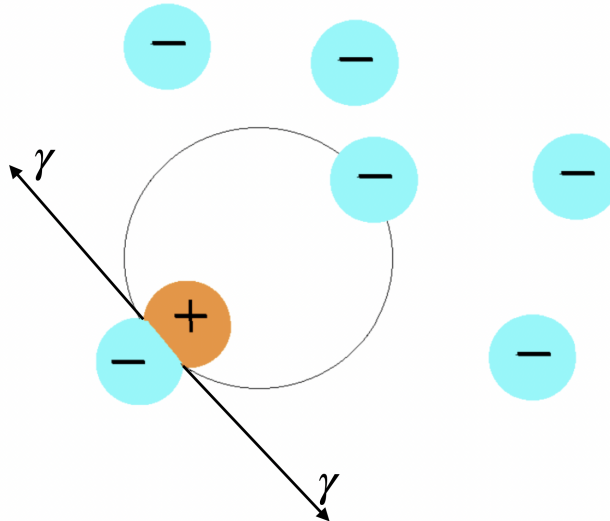


Figure 3.2: *Left*: Schematic representation of pick-off process, in which the positron forming the positronium annihilates with the electron from the surrounding matter.

The ortho-para conversion occurs when the electron comprising the positronium exchanges the spin with the electron in surrounding matter resulting in conversion of ortho-positronium into the state of para-positronium. As a result the lifetime of positronium is shortened and it annihilates into equal number (most often two) gamma quanta. This process is likely to occur in presence of paramagnetic molecules, such as O_2 and NO , and ions with unpaired electron. Thus the presence of such molecules in biological systems can impact the lifetime of the positronium [37].

3.2.1 Pick-off models

The model describing relation between the size of free volumes and pick-off process probability was first devised by Tao and modified by Eldrup [36, 41]. According to this model the positronium is localised in a spherical void of radius R . The positronium trapping in void is represented by the rectangular potential well with radius $R_0 = R + \Delta$. The boundary conditions are applied, that outside of that well the positronium wave function is equal to zero:

$$\begin{aligned}\Psi_{Ps,out}(r_0) &= \Psi_{Ps,in}(r_0), \\ \Psi'_{Ps,out}(r_0) &= \Psi'_{Ps,in}(r_0), \\ \Psi'_{Ps,in}(r_1) &= 0,\end{aligned}\tag{3.3}$$

where U_0 is initial value of the potential, r_0 is the radius of barrier representing the molecular forces in the medium, r_1 is summary radius of the well and barrier, $\Psi_{Ps,out}$ and $\Psi_{Ps,in}$ are positronium wave functions outside and inside the well [36].

The parameter Δ is the region in which positronium wave function inside the well partially overlaps with the electron cloud around the void. In this layer the pick-off process can occur. The value ΔR was empirically established to be 0.166nm for small voids in

organic media [42]. The Tao-Eldrup model is good at description of empirically observed data of positronium lifetimes e.g. in case of vacancies in plastic crystals, with relatively large spherical voids.

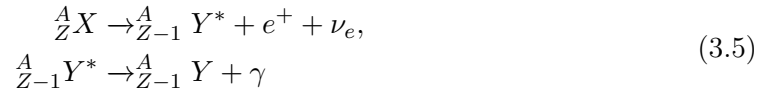
The relation described by Tao and Eldrup for probability of positronium annihilation due to the pick-off process is described as:

$$P = 1 - \frac{R}{R + \Delta} + \frac{1}{2\pi} \sin\left(\frac{2\pi R}{R + \Delta}\right) \quad (3.4)$$

The Tao-Eldrup model was further modified by other scientists towards extending the scope of its applications. To fit the observations for media characterised by ellipsoidal voids the model was extended by Jean [43] and for the free volumes with elongated vacancies the model was proposed by Goworek [44]. The pick-off process is the main regime of positronium annihilation in most media, and the above model can be applied for calculations of sizes of free volumes in specific materials based on the measurements of positronium lifetime in a technique called Positronium Lifetime Spectroscopy (PALS).

3.3 Positronium Annihilation Lifetime Spectroscopy

Positronium Annihilation Lifetime Spectroscopy (PALS) is a useful tool for the studies of inter- and intramolecular structure of various materials. It has been shown, that this method of examination, may also be useful in bio-medical studies of differences between healthy and malignant tissues, as delineated in section 3.5. This technique uses radioactive isotopes that produce $\beta+$ particles and additionally emit a prompt gamma quanta that originates from deexcitation of daughter nucleus. This type of $\beta+$ decay can be described as:



where A denotes mass number and Z atomic number of the atom, X is a parent nuclide, Y^* is daughter nuclide in excited state, e^+ is a positron, ν_e is an electron neutrino, Y is daughter nuclide in ground state, γ is gamma quantum emitted in process of deexcitation. An example of such isotope is ${}^{22}\text{Na}$, which decay scheme is illustrated in Figure 3.3.

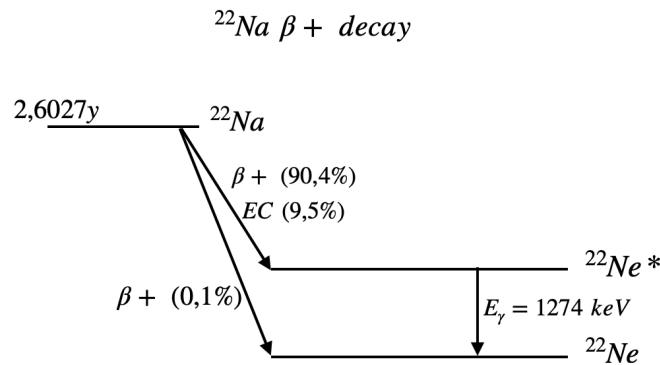


Figure 3.3: The ${}^{22}\text{Na}$ isotope decay scheme. This isotope undergoes $\beta+$ decay into neon in excited state with emission of positron with 90.4% probability. Shortly, the neon undergoes deexcitation with emission of gamma quanta with energy of 1274 keV.

The measurement of a positronium lifetime is done with assumption that the time of emission of deexcitation gamma quanta, which the detector registers, is happening almost exactly at the time of formation of positronium in matter. The time it takes for the isotope to undergo deexcitation and emit gamma quanta, which, in case of ^{22}Na , has energy of 1274 keV, is approximately the time that is needed for the positron to thermalise. A positron loses its kinetic energy by the means of ionising the surrounding molecules along its track, and then it combines with electron to form a positronium. This processes happen in the order of picoseconds while the measured lifetime is in the order of nanoseconds. Once positronium has formed in matter, its lifetime, compared to vacuum, may be shortened due to the processes such as pick-off process or ortho-para conversion. As a result it annihilates into two gamma quanta in angle near 180° with energies of 511 keV, which may be registered by the detector. The slight deviation from this values can occur due to the greater than 0 net momentum of the positronium. The described order of events in singular lifetime measurement is shown in Figure 3.4.

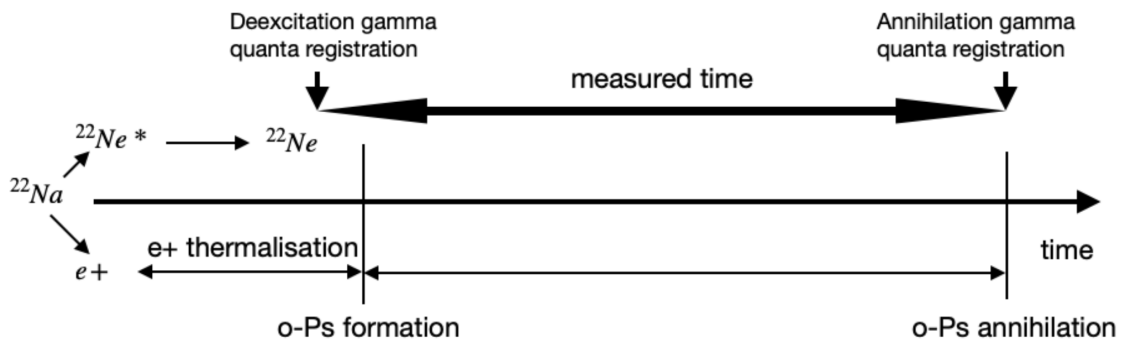


Figure 3.4: The order of events in singular positronium lifetime measurement. The ^{22}Na decays into $^{22}\text{Ne}^*$ and emits a positron into the sample. After short period of time the positron forms positronium (e.g. ortho-positronium) while ^{22}Ne emits deexcitation gamma quanta, which registration marks the start of singular lifetime measurement. When positronium undergoes annihilation it emits annihilation gamma quanta, which registration marks the end of singular lifetime measurement. In other words, lifetime of positronium is measured as a difference of times between registration of annihilation and deexcitation gamma quanta.

3.4 Positron annihilation in metals

As opposed to porous molecular media, in metals there is little to no positronium formation occurring due to the high electron density of metals. In perfectly formed metal lattice the positrons are delocalised and can be represented as a periodically extended Bloch-like states, with positron density lowest at the positively charged ion cores of the atoms and highest at the interstitial regions. The measurement of mean lifetime of positron in metal yields information about total electron density [31]. The net positron lifetime should be equivalent between defect-free lattices of the same metals. In actuality the internal structure of metal is dependent on the method of production (e.g. quenching) during which lattice defects may develop, such as vacancies, vacancy clusters etc. In such defects positrons can appear as highly localized bound-states, and thus the presence of defects can lengthen the mean positron lifetime in the sample [45, 46].

According to the trapping model positrons are trapped by defects immediately after thermalisation. They will annihilate with rate λ_c in perfect crystal region (rate of positrons annihilation in bulk or Bloch state) and with smaller rate λ_t if they are trapped in lattice defects [47]. The relationship between the annihilation rate λ and observed lifetime τ of positrons is described by:

$$\tau = \lambda^{-1} \quad (3.6)$$

The lifetime spectrum attained during the positron annihilation measurement is a sum of exponentially decaying components corresponding to types of trapping sites. Analysis of such spectra can yield information about the shape and concentration of the defects in crystalline materials.

In given metal sample there may be multiple components corresponding to lifetimes of positrons trapped in deformities. In case of metal lattice with two kinds of defects, three components can be found in the lifetime spectra: one corresponding to lifetime of positrons in bulk state and two corresponding to the lifetime of trapped positrons.

The ability to distinguish between those components depends on the resolution of the measurement setup. Without the required precision, one could nonetheless observe those components' mean lifetime value (also called average lifetime value), which can be described as:

$$\bar{\tau} = \tau_c \cdot I_c + \tau_t \cdot I_t, \quad (3.7)$$

where $\bar{\tau}$ is the mean lifetime, τ_c is positron lifetime in crystal lattice, I_c is the intensity of the crystal lattice component, τ_t is positron lifetime in defect and I_t is the intensity of the 'positron lifetime in defect' component. As the amount of the deformations in the sample drops, the observed lifetime should approach the value for positron lifetime in defect free lattice τ_c [47].

Based on this, it can be assumed, that in any pure sample of specific metal type, it would be possible to observe the mean lifetime value between the value of mean positron lifetime in metal lattice and mean positron lifetime in defects. If the same sample of metal would be measured in different setups, the observed lifetime values should be equivalent in between the measurements. The differences in spectra would arise only due to the different timing resolutions of the detection systems.

The positron annihilation measurement is a tool used in material science for studying structure defects in metals. There are multiple studies describing the empirically determined values for the positron lifetimes in samples with various types of defects. There are models, as a trapping model described above, aiming to describe the empirical data. Some researchers have performed calculations to asses the value of the positron lifetime in defect-free lattice of certain materials based on the lattice structure and properties. The bulk value of positron annihilation in copper was calculated to be equal to 110 ps, the value of τ_c for nickel was calculated to be 110 ps and for aluminum the τ_c value was calculated as 163 ps [48].

In empirical study, in which researchers observed two components in copper sample, the positron lifetime values are $\tau_c = 122(5)$ ps and $\tau_t 176(5)$ ps [49]. Another reaserch group has found similar results, with mean value of their sample determined as 158 ± 1.5 ps [50].

An example of empirically found value of $\bar{\tau}$ for nickel samples prepared at low (25 mA/cm^2) current density and annealed in temperatures between 50 to 250°C was found to be around 160 ps [51]. The lifetime values grow with rising annealing temperatures, which points to voids growth with heating, and later drop above 450°C [52].

In experimental study, researchers have found the positron lifetime values to be 161 ± 2 ps for τ_c and 243 ± 1 ps in monovacancy trap for aluminum that was alloyed in between

(and including) 200 and 400°C [53]. These findings are summarised in Table 3.1.

Table 3.1: Literature values of positron lifetime in aluminum, copper and nickel both calculated and empirically found. The calculated lifetime refers to the positron annihilation in metal’s pure lattice. τ_c is the lifetime value determined for positron annihilation in metal lattice by empirical study, τ_m is the lifetime value determined for positron trapped in monovacancy, $\bar{\tau}$ is the measured value of mean positron lifetime.

Element	Calculated [ps]	Empirical [ps]
Aluminum	163 [48]	$\tau_c = 161 \pm 2$, $\tau_m = 243 \pm 1$ [53]
Copper	110 [48]	$\tau_c = 122(5)$, $\tau_m = 176(5)$ [49] $\bar{\tau} = 158 \pm 1.5$ [50]
Nickel	110 [48]	$\bar{\tau} = 160$ [51]

3.5 Positronium imaging in medical diagnostics

The phenomenon of positron annihilation allows us to study internal structure of various inorganic materials [54], but it also can be a tool for examination of biological matter as proposed in [2, 11].

The current state of knowledge on positronium behaviour in organic matter shows interesting dependencies between positronium annihilation rate and the disease, yet there is still a necessity for continued investigations in view of biological and medical applications to predict the positronium behaviour in wider range of diseases. Learning the properties of positronium in biological matter will allow for creating the database for positronium imaging diagnostics with common references for various types of detection systems.

This chapter presents a few of those studies that focus on the positronium lifetime properties in tissues, cells and body fluids that were performed up to this date. Studies presented here explore positronium lifetime in view of investigating the dependency of lifetime on various factors and have employed living cells and tissues in their inquiries.

3.5.1 Positronium in cancer

Cancer is a group of diseases that are characterised by abnormal cells growth. Some of the cancer diseases constitute of neoplastic growths, which are created by the uncoordinated proliferation of the tissues creating tumours.

The cells that constitute a tumor are descendants of a cell, which at some point underwent series of mutations of the proto-oncogenes and tumor suppressor genes. Invariant to normal signalling pathways that regulate the life-cycle of the cell, cells can excessively proliferate, eventually forming malignant mass. The cells leaving the initial tumour may form metastases in the human body that become dangerous for proper functioning of the vital organs and may eventually lead to death [55].

PET imaging is an effective tool for cancer diagnostics allowing for insight into biochemical and physiological changes in the body that precede the structural changes, thus permitting an earlier detection of diseases. Accompanied by computer tomography (CT), a technique based on structural imaging, it allows early detection of cancer, the metastasis and plays an important role in cancer staging and treatment monitoring.

Despite its effectiveness, PET imaging is yet not able to provide with information about the chemical environment and molecular composition of the affected region, while, in some

cases, this knowledge could impact the decisions undertaken by the medical professionals in creating a treatment plan.

It has been observed that some of the cancer cells exhibit a higher oxidative stress levels compared to healthy cells [56]. The mechanism of free radicals accumulation is based upon the mitochondrial dysfunction of the cancer cells, one of the ways is due to a low coupling efficiency of the mitochondrial electron transport chain, which in turn raises electron leakage and increases the rate of reactive oxygen species (ROS) formation. Additionally to that, the antioxidant system functioning is reduced in cancer cells. This setup works two-fold: the elevated ROS levels can lead to further damaging the cancer cells and producing more mutations, that may lead to the advance of the disease, on the other hand the tumor cells become more vulnerable, and there even are strategies that use this phenomenon to kill off cancer cells in a method called "oxidation therapy" [57]. This two processes are usually prevalent in different stages of the disease. During the early stages of tumor growth the ROS appear to promote cancer initiation via inducing oxidative damage and mutation. ROS seem to play opposite role at the later stages of tumor growth, when their accumulation influences apoptosis of the cancer cells, which in turn produce intracellular antioxidants to prevent them from oxidative injuries. Depending on the stage and course of the cancer the medical professionals have to apply different treatment plans [58], such as e.g. hypoxia sensitive chemotherapy [59]. That is one of the reasons for the development of positronium imaging technique, which could show to be beneficial in sensing the levels of ROS and free radicals. Due to the tendency of the diseased tissue to permeate elevated ROS levels, it is anticipated that the lifetime of free positrons will be shortened compared to the healthy tissues [60].

Set of studies show that ortho-positronium mean lifetime is correlated with the grade of development of metabolic disorders in cancer cells by the means of sensing the degree of hypoxic states [61, 62]. This studies were done using the model environment, which comprised of the water samples with different oxygen partial pressure values. In one study it was shown that there is good linear correlation between pO_2 value and positronium lifetime, and they achieved resolution of 10 mmHg, which allows for distinction between healthy liver tissue and hypoxic liver tumours. It was established that the presence of oxygen does not affect the lifetime of free positrons [62].

The value of the positronium lifetime and its intensity, as one would expect, is not identical for all types of abnormal growths. Tumours originating from different tissues are distinct from each other as well as from the healthy tissues. An example of that may be benign neurofibromas having more diffusive appearance than malignant peripheral nerve sheath tumours, that are densely packed cell clusters [55]. This in turn can result in smaller electron free volumes and raised rate of positron annihilation due to the pick-off process.

Comparing the positronium annihilation in human basal cell carcinoma and squamous cell carcinoma with normal skin cells researchers have noted that cancer cells stand apart from healthy cells by shorter o-Ps lifetime and lower o-Ps intensity, which point to higher rate of positron annihilation that may emerge due to higher concentration of free radicals or other reactive molecules and/or reduction of free volume size [63, 64].

In later study of different type of skin cancer, researchers have observed that for melanoma cells the intensity of o-Ps is indeed lower, as it was in case of previous study SCC and BCC, but the lifetime value for o-Ps did not differ significantly from that of normal cells, while pointing out that the lack of difference may come from lower concentration of melanoma cells used in the study. Authors proposed a concept of different method of more controlled and systematic study employing UV-induced skin cancer in vivo derived from living animals [7].

The internal structure and molecular composition of cancerous growth may change depending on its stage. The key to employing the positronium imaging method in clinical setup lays in learning the relations between the changes in positronium lifetime values and stages of development of malignancy. The later study of melanoma cells has shown that for diseased tissues the ortho-positronium lifetime values are significantly larger and the intensities are higher compared to healthy melanocytes. The free positron lifetime values have also shown to be higher than for healthy tissues. The observed differences were significant not only between the healthy and cancerous tissues, but also between the cancerous melanoma cells with different degrees of malignancy pointing to the applicability of the method to detect the disease progression [8]. The differences in o-Ps lifetimes around 100 ps and intensities around 4-5% presented in the study may be an example of precision required of the detectors that are to be applied for the means of medical diagnostics.

Study with uterine leiomyomas has shown that the free annihilation and ortho-positronium lifetime values were larger for the diseased tissues with respect to the lifetime for the healthy ones. The intensity of both components, generally, was found to be smaller for altered tissues than for the normal ones [5].

A 3D in vitro cell culture of colorectal cancer has been employed as a study model to prove the applicability of PALS to detect changes in molecular composition and structural changes in cancer cells as they may be accompanied by atomic scale changes in the free volume void size. The PALS measurements were conducted on different days of the cell culture growth. It was found that the PALS measurements are indeed a capable tool for detection the changes in the nanostructure, that are reflected by changes in lifetime of o-Ps. The results have shown that values of o-Ps lifetime were longer in cancer cell culture than in control cell culture up to about a month of growth time. After that the o-Ps lifetime in cancer cell growth were characterised by shorted o-Ps lifetime, which may result from the cell death [65].

In contrast to those findings, studies that used cancerous colon tissue acquired from hospital patients done at Jagiellonian University did not prove to be there unequivocal differences between ortho-positronium lifetime in healthy and diseased tissues [66].

The ex vivo study of formalin-fixed benign tumor of cardiac myxoma conducted with PALS technique had shown the mean value of o-Ps lifetime to be 2.01(02) ns with observed differences of the 10 measured samples to be about 20 ps in lifetime value and 1% in intensity which proved a consistency in results between the samples originating from different patients. Additionally 5 samples were measured without the fixation and results were compared with values obtained for adipose tissue. Significant differences were observed between the two, with significantly shorter o-Ps lifetimes and lower intensities observed for benign tumor than for the adipose tissue [8].

The first ex vivo study done with J-PET detector has employed the cardiac myxoma and adipose tissues for proving that the positronium image is possible to obtain with J-PET detector. In this study two of each types of unfixed tissues were placed inside the scanner with the ^{22}Na sources. Both the standardised uptake value as well as the lifetime spectra were obtained. After the spectra analysis the significant differences were found between the positronium lifetime values for benign tumor and healthy adipose tissue [3], in accordance with results of PALS study [8].

3.5.2 Other applications in medicine

Alongside the studies of cancerous tissues, the Positronium Lifetime Spectroscopy can be used in research of various other diseases.

It was proposed that measuring positronium lifetime can be useful in diagnosis of

cardiovascular diseases. Studies of feasibility of positronium application for blood clots structural characteristics are currently being conducted at Jagiellonian University [67]. Blood clotting is a process that is at the service of maintaining the homeostasis of the body, preventing life-threatening haemorrhages and a part of tissue repair process, albeit a pathological blood clot formation may lead to fatal events, such as e.g. stroke. The possibility of not-invasive blood clot examination is an incentive for the studies done currently at the Jagiellonian University.

Distinct study that concentrated on different techniques of measurements of Extracellular Vesicles (EVs), including PALS technique, gave insight on ortho-positronium lifetimes in EVs, which are lipid-bound vesicles secreted by various cells into the extra-cellular space, which play a role in cell-to-cell communication and have the potential to be used as drug transporters and biomarkers [68].

The PALS measurements have been employed in other fields of biology, e.g. examination of brewing yeasts allowed for observations of dynamic of water sorption of those cells by evaluating the sizes of free volumes [30], PALS has also been used to analyse the porosity of the bone and molecular changes in human hair subjected to UV exposure [69, 70].

In summary, the mean lifetime and intensity of the positronium depend on the tissue structure, type and stage of disease and may become a biomarker used in positronium imaging technique. It was shown in empirical studies, that various samples of cancer tissue are characterised by lengthened lifetime of positron and ortho-positronium compared to healthy tissue and lower intensities for those components [5] and other studies have found the similar lifetime relationship but with higher intensities [8] as well as no significant differences between healthy and diseased tissues [66].

The stage of understanding of positronium interactions inside the matter allows researchers for creating hypotheses about processes that occur in the researched samples. Yet more studies are needed to obtain better understanding of interactions at molecular level of biological material and how they impact the o-Ps lifetime in specific type of tissue or malignancy.

3.6 Positronium imaging

The idea of positronium imaging was devised at the Jagiellonian University by professor Paweł Moskal and is currently being developed by the J-PET collaboration [4]. This new method of imaging, employing the analysis of the formation and annihilation of positronium, is complementary to the Positron Emission Tomography (PET) imaging. In classic PET imaging the detector registers pairs of gamma quanta emitted as a result of annihilation of a positron and electron. In positronium imaging it is required to register 3 photons: additionally to the two gamma quanta emitted after the annihilation a third gamma quanta is necessary, which is emitted as a result of deexcitation of an excited nucleus. The gamma quanta originating from deexcitation of daughter nucleus is called the prompt gamma. The prompt gamma quanta has a characteristic energy dictated by the size of energy difference between excited and ground states of the nucleus. To perform positronium imaging a detector must be adjusted for multi-photon detection and image reconstruction [4, 9].

A classic PET imaging is very effective tool in early detection of cancer, detection of metastases and monitoring of the treatment progress. Outside of cancer-related diagnostics PET is also used for imaging and diagnosing inflammation, neurodegenerative diseases, neurological disorders and cardiovascular diseases [71–73]. The PET imaging could benefit

from analysis of the positronium lifetime spectra, as 40% of positron annihilation, that occurs inside a human body, occurs through creation and annihilation of positronium bound state [1, 2]. It has been shown that most of those annihilations happen through the pick-off process, as a result of which two gamma quanta are emitted [62]. The impact of intra and intermolecular structure and molecular composition of the biological matter on positronium annihilation rate can become the important biomarker of diseases [1, 2, 74]. With addition of positronium imaging to the classic PET imaging it will be possible to observe not only the distribution of radiopharmaceutical but also, for a chosen voxels, to see the values of positronium lifetimes and intensities of components corresponding to different positron states that arise in the examined volume [74]. Positronium imaging could raise the specificity of the diagnosis through insight into structural and molecular composition of the regions of the body suspected be afflicted [2, 74].

One of the scanners eligible to perform positronium imaging, and the first PET scanner to have been ever used for this purpose, is the J-PET scanner [4, 9]. The J-PET scanner was devised at the Jagiellonian University with the aim of creating cost effective alternative for the PET scanners used currently in clinical settings. In contrast with classic PET detectors that comprise of crystal scintillators, the J-PET detector is build with low-cost alternative of plastic scintillators [75]. The design of the J-PET scanner places the scintillator strips along the patient body in such way that the signal is collected on the both ends of the scintillator strip, unlike in crystal PET detectors where the crystals are organised radially. The plastic scintillator are characterised by better timing properties than crystal scintillators, alas due to their lower density, they also show worse detection efficiency for the gamma quanta [9, 75].

The development of the new method of imaging requires studies of various instances that constitute into the well developed technique. The first feasibility studies were performed successfully with simulations [11]. The study has shown that using J-PET detector it is possible to obtain both the density distribution image and a mean lifetime of ortho-positronium for each voxel. The later empirical studies of positronium imaging feasibility have shown that it is possible to reconstruct the image arising from annihilation of positronium into 3 γ quanta [12].

Concurrently there were several studies performed that explored the positronium properties in biological samples by the means of Positronium Annihilation Lifetime Spectroscopy technique, some of them delineated in section 3.5. It is crucial to learn what ranges of positronium lifetime values can be observed in various types of biological tissues, both healthy and diseased. For instance ex vivo studies of cardiac myxoma and adipose tissue have shown, that there is an observable difference between positronium lifetime and intensity between those tissues [8, 13].

The positronium imaging of biological tissues has been performed with Jagiellonian-PET comparing the lifetime spectra of ex vivo tissues [13, 14]. Later, the Jagiellonian-PET has been employed to obtain the first positronium image of human brain in vivo [15]. Recently, the Biograph Vision Quadra scanner produced by Siemens Healthineers has been shown capable of performing positronium imaging with samples of quartz glass and polycarbonate [10].

3.7 Radionuclides for positronium imaging

In case of classical PET imaging the isotopes are characterised by emission of β^+ radiation, but for means of positronium imaging it is crucial that the source emits additional γ quanta after the β^+ particle is emitted, allowing for lifetime measurement described in

section section 3.3.

The isotopes that are candidates for positronium imaging in medical diagnostics must be also characterised by a range of other conditions: safety of usage by people, adequate half life (long enough for diagnostic procedure and short enough to reduce irradiation on the body after procedure). It is crucial that they produce prompt γ radiation with suitable energy for means of imaging, but also they should be characterised by high $\beta+$ branching ratio (instead of electron capture) and preferably not emit multiples of other γ -rays (to reduce background that might decrease the precision of the imaging) [76].

The most promising candidate for medical positron imaging is ^{44}Sc with as many as 94% of $\beta+$ decays undergoing with emission of prompt gamma quanta. The decay scheme of ^{44}Sc is presented in Figure 3.6. ^{68}Ga is commonly used for PET imaging, but it has very low intensity of γ suitable for positronium imaging. Its decay scheme is presented in Figure 3.5. Another example of isotope for positronium imaging may be ^{124}I . Although it has relatively low $\beta+$ branching ratio and the medium-intensive medium-energy γ line, it can be paired with therapeutical ^{131}I used for the treatment of hyperthyroidism and thyroid cancer.

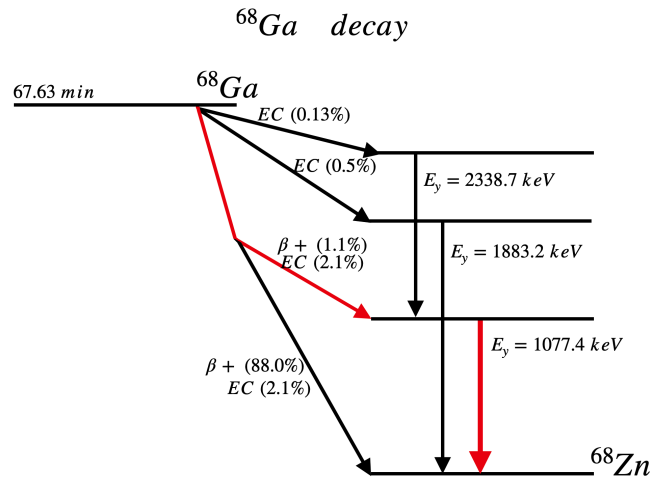


Figure 3.5: Decay scheme of ^{68}Ga . The red arrows mark the pathway in which with 1.1% probability the isotope decays into zinc in excited state and a positron is emitted. In the process of deexcitation a prompt gamma quanta with energy 1077.8 keV is emitted. Based on [77].

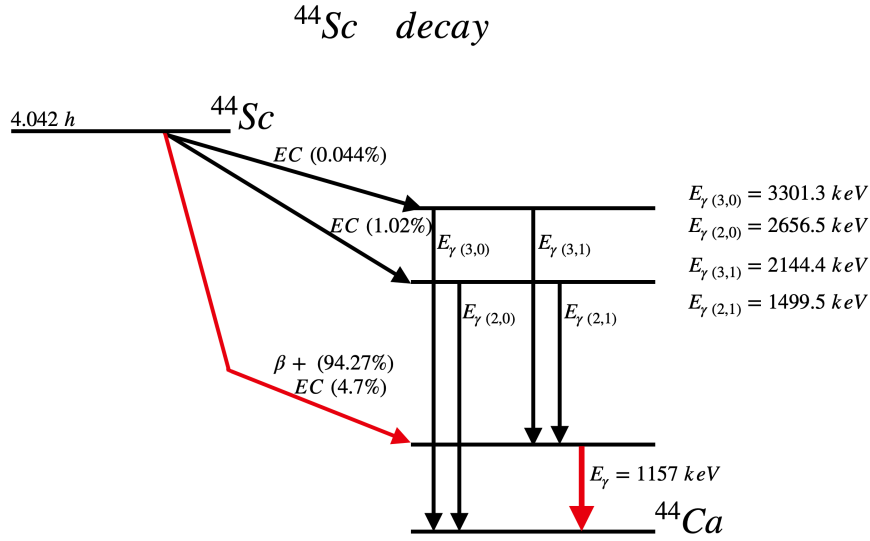


Figure 3.6: Decay scheme of ^{44}Sc . The red arrows mark the pathway in which with 94.27% probability the isotope decays into calcium in excited state and positron is emitted. In the process of deexcitation a prompt gamma quanta with energy 1157 keV is emitted. Based on [78].

3.8 Positron range

Though a positron injected into the matter may travel a small distance, the point of emission of prompt γ quanta is assumed to be the same location that is the point of emission of annihilation γ quanta. In actuality, the difference between the source location and the 511 keV γ emission point may differ depending on the stopping power of the tissue and the energy of the $\beta+$ particle.

The positron source used for PAL spectrometry and modular J-PET measurements in the course of this thesis was ^{22}Na and for the measurements with Biograph Vision Quadra, the applied isotope was ^{68}Ga . The comparison of energies of $\beta+$ particles emitted by those isotopes is presented in Table 3.2. The sodium source emits positrons with abundance of 89.8% with maximum energy of 545.5 keV and average energy of 215.5 keV. Alternatively, with abundance of 0.6% it emits positrons with maximum energy of 2842.1 keV and average energy of 834.8 keV. For ^{68}Ga isotope the energies of the positrons that are available for positronium imaging purposes (they constitute only 1.1% of all emissions) have maximal energy of 821.7 keV and average energy of 352.6 keV.

Table 3.2: Energies of $\beta+$ particles emitted by the ^{22}Na and ^{68}Ga isotopes.

Isotope		$\beta+$ energies	
		Max. energy [keV]	Avg. energy [keV]
^{22}Na	Abundance 89.8%	545.5	215.5
	Abundance 0.6%	2842.1	834.8
^{68}Ga		821.7	352.6

Based on equations:

$$r = 0.412 \cdot E^{1.27-0.0954 \cdot \ln E}, \quad (3.8)$$

and

$$X = \frac{r}{\rho} \quad (3.9)$$

where r is the positron range and E is the positron energy in MeV, X is the positron mean free path and ρ is material density, the maximum and average ranges were calculated for air and examined disk materials [79]. Average and maximum range for the positrons from the ^{22}Na injected into materials that constituted the examined disks is presented in Table 3.3, while Table 3.4 contains similar information for ^{68}Ga .

Table 3.3: Maximum and average range of positrons in air and disk materials for positrons emitted by ^{22}Na source [80].

Material	89.8% abundance		0.6% abundance	
	Max range [mm]	Avg range [mm]	Max range [mm]	Avg range [mm]
Air	1417.2	360.4	12686.5	2493.58
Aluminum	0.68	0.17	6.10	1.20
Nickel	0.21	0.05	1.85	0.36
Copper	0.21	0.05	1.84	0.36
Quartz	0.70	0.18	6.22	1.22

Table 3.4: Maximum and average range of positrons in air and disk materials for positrons emitted by ^{68}Ga source [80].

Material	Max range [mm]	Avg range [mm]
Air	2698.02	740.29
Aluminum	1.30	0.37
Nickel	0.39	0.11
Copper	0.39	0.11
Quartz	1.32	0.37

The ranges presented in the Tables 3.3 and 3.4 point to conclusion that the positrons from decay of ^{22}Na isotope with abundance of 89.8 % are fully stopped inside 1mm thick disks of presented materials. Positrons with maximal energy are stopped by 2 cm thick layer of copper or nickel and 6.5 cm thick layer of aluminum or quartz glass.

The β^+ particles emitted by ^{68}Ga will be stopped by the disks with 1.5 cm thickness.

3.9 Exemplary positronium detection systems

A scanner eligible for the positronium imaging must be suited for time difference measurements and in addition to the ability to detect annihilation gamma quanta with energies of 511 keV it must register prompt gamma quanta with higher energies [4, 9]. This type of setup, similarly as described in section 3.3, has to be able to detect and identify the deexcitation and annihilation gamma quanta falling inside the coincidence window and have good timing resolution to be able to accurately determine the time differences between registered photons. A coincidence is a registration of at least two interactions within a detector in specified time interval, named the time window.

A system used for measurements of the time difference between registration of de-excitation and annihilation gamma is the PALS, which consists of two detectors placed axially. Each detector consists of crystal scintillator and photomultiplier. In most of the PALS systems and common PET detectors the photons are detected by the means of crystal scintillators and the selection of correct coincidences, where deexcitation and annihilation photons are registered within specific time window, is based on the photoelectric effect [81].

In photoelectric effect the quantum of radiation transfers entire energy to an inner shell electron of an absorber atom, this electron is ejected from the atom with kinetic energy equal to the difference between the energy of gamma photon and binding energy of that electron.

The photoelectric peak allows for applying clear condition for choosing the energy windows for the start and stop signals in time difference measurements. However, the costs of crystal scintillators in amounts and quality needed for producing a PET scanner are very high comparing to a two-detector setup, like PALS. The costs of purchase and maintenance are an important factor limiting the availability of the PET medical diagnostics.

It was proposed at the Jagiellonian University that the PET scanner can be made out of plastic scintillators characterised by their low prize comparing to the crystals. This state-of-art concept would allow for reducing the prize of the production of the detector, translating into more affordable alternative to the crystal PET systems [9]. Such scanner, additionally to performing the classic method of PET imaging, can also be applied for the positronium imaging. The plastic scintillators are produced from low Z materials, and as a result the main mechanism of interaction of gamma quanta with this type of detector is by Compton effect, in which the gamma quanta transfers only a part of its energy to the electron from the outer shell, resulting in ejection of this electron with certain energy and momentum and scattering of the photon. Due to the low Z value of the material the photoelectric effect is negligible in organic scintillators.

The light produced inside the scintillator is converted into electric signal by the photomultipliers attached to them, for example by the means of optical gel.

In PALS systems the complying scintillators must be characterised by good timing properties. The types of crystals used in PALS setups are BaF_2 , which stand out with its very short decay time of about 0.6 ns [82].

The PET systems make use of crystal scintillators such as LSO, excelling with their high light output and stopping power, with scintillation decay time of about 40 ns. This type of detector is characterised by high natural background due to ^{176}Lu emitting photons with energies in range of 88 - 800keV [10].

Compared to crystal scintillators, plastic scintillators are characterised by low stopping power and low energy resolution, but high timing resolution: short decay time and raise time [83]. As such they may be well fit for production of the time-of-flight scanners, such as the one used for the study presented in this thesis [75].

In Table 3.5 there is a comparison between the properties of scintillators used in all detection systems used in this study.

Table 3.5: Comparison of the properties of the BaF_2 scintillators [82, 84] used for example in PALS setups, BC-404 plastic scintillators [83] used in Modular J-PET and LSO scintillators [85, 86].

Name	Light output [photons/keV]	Light Attenuation Length [cm]	Rise Time [ns]	Decay time [ns]	Density [g/cm ³]
BaF_2	10 (Slow) 1.9 (Fast)	-	<0.004	630 (Slow) 0.8 (Fast)	4.88
BC-404	10.4	140	0.7	1.8	1.032
LSO	30	1.14	0.7	40	7.4

4. Experimental methods

This chapter focuses on the measurement procedures, descriptions of the measurement setups and analysis of the data that will allow for positronium lifetime spectra extraction.

The study presented in this thesis was done with use of three detection systems, that differ both in hardware and software used to detect and analyse the data from positron annihilation: Positron Annihilation Lifetime Spectroscopy, modular J-PET and Biograph Vision Quadra. The PAL spectroscopy at Jagiellonian University consists of detectors with BaF_2 crystal scintillators and tube photomultipliers.

The modular J-PET scanner uses plastic scintillators and is intended as an alternative to a classic PET scanner that uses crystal scintillators. Good timing resolution of plastic scintillators situate it as a candidate for positronium imaging detector [75]. This scanner uses silicon photomultipliers (SiPMs), which have an advantage of smaller size, immunity to magnetic fields, low operating voltages and high photon detection efficiency in comparison with tube photomultipliers [87].

The third system shown in this study is Biograph Vision Quadra PET/CT scanner produced by Siemens Healthineers. This detector, which is qualified for clinical use, is also shown to be a good tool for positronium imaging. This tomograph consists of lutetium-oxoorthosilicate (LSO) crystals coupled with silicon photomultipliers (SiPMs) [25]. The experiments at the Inselspital in Bern were done thanks to the collaboration with Prof. Axel Rominger, Prof. Kuangyu Shi, Prof. Ewa Stepień, Prof. Paweł Moskal and Dr William Steinberger.

Described detection setups are presented in Figure 4.1.



Figure 4.1: *Left:* The PALS setup in Jagiellonian University, Kraków. *Middle:* Modular J-PET scanner in Jagiellonian University, Kraków. *Right:* Biograph Vision Quadra PET/CT scanner in Inselspital in Bern, Switzerland.

The timeline of the measurements is presented in Figure 4.2. The more detailed dates and measurements duration times are described in respective chapters.



Figure 4.2: Timeline of the measurements. The measurements took place over the course of eight months in year 2023. The first measurement was done at Inselhospital in Bern on 27th of February and carried on for 1 hour. The Positron Annihilation Lifetime Spectroscopy (PALS) measurements were performed in span of two and a half months. They consisted of 17 measurement that lasted up to 21.5 hours. The measurement done with modular J-PET scanner carried on for 24 hours and took place on 19th through 20th of July (in between the PALS measurements).

Table 4.1: Comparison of characteristics of the PALS, Modular J-PET prototype and Biograph Vision Quadra detection systems.

Detector	PALS	Modular J-PET	Quadra
Scintillator	BaF_2	BC-404 plastic	LSO
Light sensor	PM	SiPM	SiPM
Axial length	—	50 cm	106 cm

4.1 Sources

The sources used in the course of this thesis for lifetime measurements with PALS and J-PET scanner were ^{22}Na sources. Those sources are characterised by a long half lifetime of about 2.5 year. The source is a small drop of sodium isotope affixed between the kapton foils that are later glued together. To secure it for the measurements with biological tissues, that are done in the same laboratory, it is additionally encapsulated inside a thin layer of Parafilm, prepared by stretching it out, before coating the source. The scheme of source structure is presented in Figure 4.3. This protective layers also allow for attaching the source to the rings of the measurement chamber that are used, among others, for biological studies. The sources are presented in Figure 4.4. Their respective activities are given in Table 4.2.

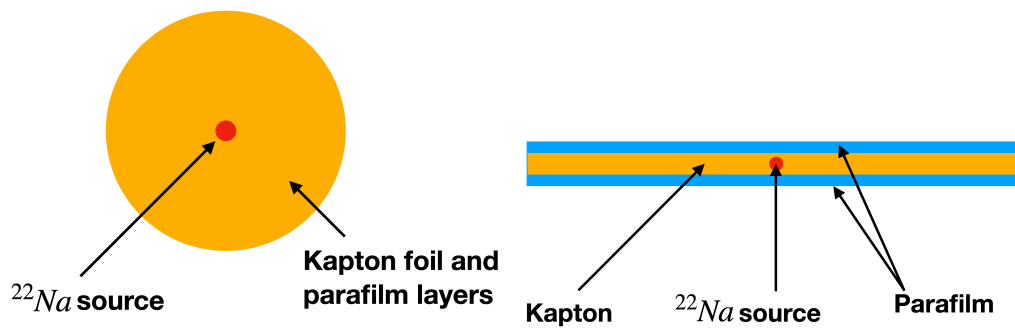


Figure 4.3: Schematic depictions of the source's structure. The red dot represents the ^{22}Na isotope placement. *Left:* The source projection from the above. *Right:* The side cross-section of the source.

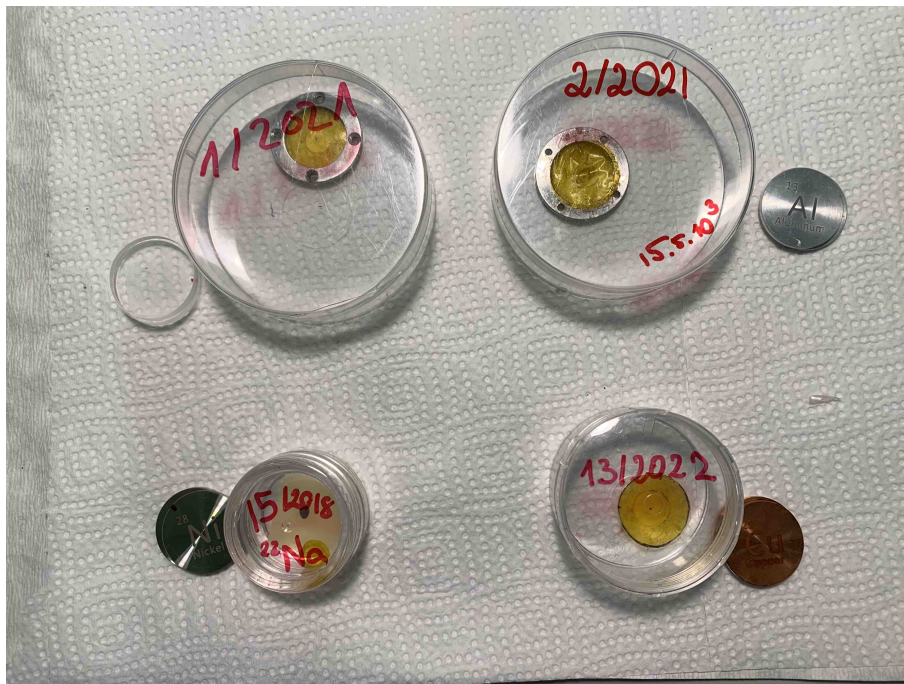


Figure 4.4: Sources used in the measurement. The sources 1/2021 and 2/2021 are attached to aluminum rings, which are a part of measurement chamber used in the lab for measurements of loose materials or biological samples. The rings were not removed for duration of the measurement in J-PET scanner. Visible on the bottom left, the source 15/2018 has no Parafilm layer and has a smaller circumference of kapton layer than the rest of the sources. The source 13/2022 on the bottom right, is removed from the ring and has been used in all PALS measurements with the disks sent by doctor William Steinberger.

Table 4.2: Sources with their respective activities measured on July 19th (the day of the measurement in J-PET scanner). The activity measurements were performed with Nuviotech ISOMED 2010 Dose Calibrator [88]. The last column presents disks pairings with sources for the measurement in modular J-PET scanner.

Source name	Activity [MBq]	Disks material
2/2021	0.838	Aluminum
13/2022	0.664	Copper
15/2018	2.335	Nickel
1/2021	0.917	Quartz

The 13/2022 source was used for the means of PALS measurements of the disks provided by Siemens. The source 2/2021 was additionally used in the process of establishing the values of constant components of the spectra described in section 5.3.

The positron source used during the measurement with Biograph Vision Quadra was ^{68}Ga radioisotope solution prepared with GalliPharm $^{68}\text{Ge}/^{68}\text{Ga}$ generator by Eckert & Ziegler Radiopharma GmbH. Directly before the measurement the drops of solution were placed in between the disks pairs with activity of approximately 5 MBq per disk pair.

4.2 Samples

Samples used for this study were disks of high purity of 3 types of metals (copper, aluminum, nickel) and quartz glass. The disks were provided by the Siemens associate [89]. In Figure 4.5 are the pictures of the disks used in all measurements. In Table 4.3 there are dimensions of the disks. The thickness of the disks are, according to calculations described in section 3.8, enough to stop $\beta+$ particles emitted by the ^{68}Ga source, though as a drop of radioisotope solution was administered between the disks, there was possibility of spillage around the samples.

The $\beta+$ particles from decay of ^{22}Na isotope emitted with 86.6 % of abundance are fully stopped by the disks, the particles from radiation with 0.6% abundance are stopped on average by the disks, but the maximum range of those positrons indicates that of some positrons can escape from the sample.



Figure 4.5: Pictures of the disks used in the study made of 4 different materials. *Top left to right:* Quartz and copper disks. *Bottom left to right:* Aluminum and nickel disks. The graduation scale of the caliper is 1 mm.

Table 4.3: Dimensions of disks used in the measurements. The thickness was measured using caliper with 0.01 mm precision, the diameter was measured with a ruler with 1 mm precision.

Disk material	Diameter [mm]	Thickness [mm]
Copper	25	1.78
Aluminum	24	1.83
Nickel	24	1.80
Quartz	24	4.04

4.3 Measurements with Positronium Annihilation Lifetime Spectroscopy

4.3.1 Experimental setup

A diagram of the PALS setup is presented in the Figure 4.6. Two detectors consist of Scionix BaF_2 crystal scintillators connected with H3378-51 Hamamatsu photomultipliers and are powered by CAEN SY4527 high voltage power supply. Due to the differences in detectors gain, the voltages applied to the photomultipliers were 2500 V for the detector collecting signals induced by annihilation gamma quanta and 2320 V for the detector collecting signals produced by the deexcitation gamma quantum. During a measurement

the signal from the detectors was passed to the LeCroy 608C constant fraction discriminator where the thresholds were applied: -92.3 mV and -29.3 mV for deexcitation and annihilation gamma quanta, respectively. The coincidence time window set on coincidence module LeCroy 622 was equal to 110 ns. From the coincidence module the signal was passed to the DRS4 evaluation board and saved on the local computer.

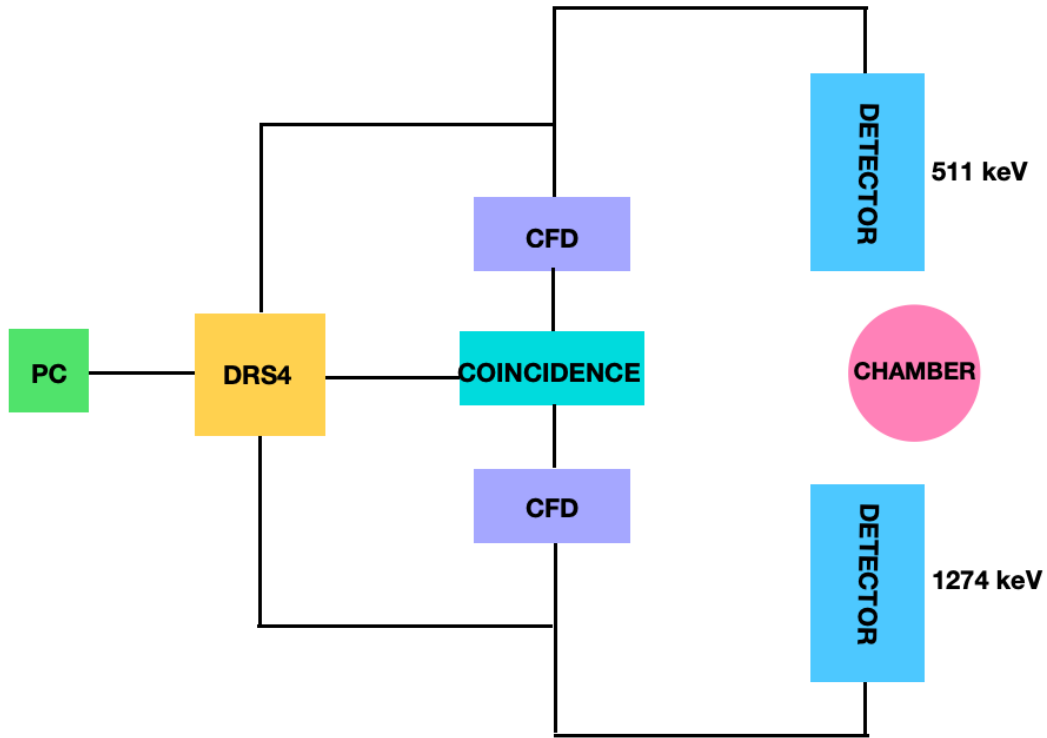


Figure 4.6: Diagram of the PALS measurement setup. The chamber (pink) that contains the β^+ source and the sample is placed off the axis of the detector to geometrically prevent registration of both annihilation gamma quanta. The detectors (blue) are set to register the annihilation gamma quanta (upper) and deexcitation gamma quanta (lower) during the measurement thanks to the respective thresholds set on Constant Fraction Discriminator (CFD, purple). The signal is passed to the coincidence module (COINCIDENCE) with time window set to 110 ns and then to DRS4 evaluation board (DRS4, yellow) and to the computer (PC, green), where the data is stored on the disk. During the lifetime measurements the signal is passing through the coincidence module, however, during the calibration measurement, the signal passes straight to the evaluation board. Both pathways are marked on the graphic.

4.3.2 Sample preparation

The source used for the measurements was ^{22}Na 13/2022 source. Around the time measurements took place the activity of the source was 0.664 MBq. The source activity was measured with Nuviatech ISOMED 2010 Dose Calibrator [88].

In the Figure 4.8 there are the pictures showing the placement of the ^{22}Na source and the samples in the PALS setup. During the measurements the source is placed between

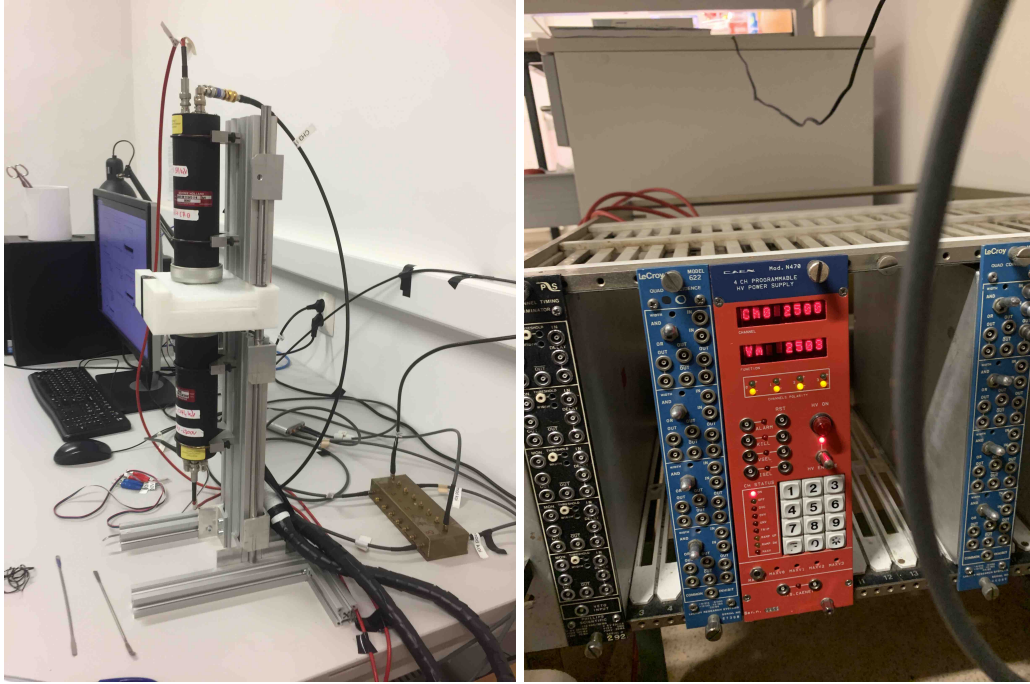


Figure 4.7: Pictures of the measurement setup. *Left:* Detectors, measurement table and PC. *Right:* CAEN SY4527 high voltage power supply and LeCroy 622 coincidence module.

the disks. The holder table is constructed in such way that the source is shifted from the center of the axis to prevent the both annihilation gamma quanta from reaching the detectors, therefore allowing for registration only pairs of deexcitation and annihilation gamma quanta. The source, the disks and the holder were marked with red marker, so that during the measurements the sample would be placed in the same manner each time.



Figure 4.8: *Upper row:* The placement of the source in between the disks. *Upper right:* The disks with the source were then placed inside the teflon chamber lower part. This enabled securing the sample in the holder table. *Bottom:* The placement of the sample in the holder table. The source and disks were always placed in the same manner thanks to the red markings on them and the table. The source is situated off the detector axis to geometrically prevent both annihilation gamma quanta from being registered. The detector visible on the picture was lowered to level of the table for the duration of the measurement.

4.3.3 Measurements

The measurements were performed on 17 different dates: one probationary measurement of nickel disks and 4 measurements per each of 4 disk materials. During the first probationary measurement of nickel disks 1 million events was collected. During the 16 subsequent measurements 4 million events per measurement were collected. An event is defined here as a registration of deexcitation gamma quanta and annihilation gamma quanta falling within the time window of 110 ns. Dates of the measurements are presented in Table 4.4. The measurements took about 12 hours each for metals, whereas for quartz glass the measurements lasted around 21 hours each. The time of the measurement depends on the rate of acquisition, which depends on the activity and slight differences in source placement inside the setup.

Table 4.4: List of the measurements with disks.

Disk material	Measurement date
Aluminum	03.07.2023
	26.07.2023
	01.08.2023
	08.09.2023
Copper	24.07.2023
	28.07.2023
	05.09.2023
	19.09.2023
Nickel	04.07.2023
	25.07.2023
	18.09.2023
	20.09.2023
Quartz	05.07.2023
	27.07.2023
	31.07.2023
	06.09.2023

4.3.4 Signal analysis

The raw data from the measurement was stored in binary format. To extract the list of lifetime differences the program Read Binary was used that was written by a member of the J-PET group doctor Kamil Dulski [90].

Information about charge, amplitude, pedestal, rise time and time at voltage threshold was acquired from the signal probed in time domain as it passed to the DRS4 evaluation board. The amplitude of the signal was calculated according to the equation:

$$A = A_{min} - Ped, \quad (4.1)$$

where A_{min} is minimal value of the spectrum, Ped is pedestal value of the signal, that was calculated as a mean value for 10 points after first 20 points from the left side of the spectrum. Information about pedestal and amplitude of the signal is crucial for calculations of the area of the signal and time at given threshold.

The exemplary charge spectra registered by one of the detectors is shown in Figure 4.9.

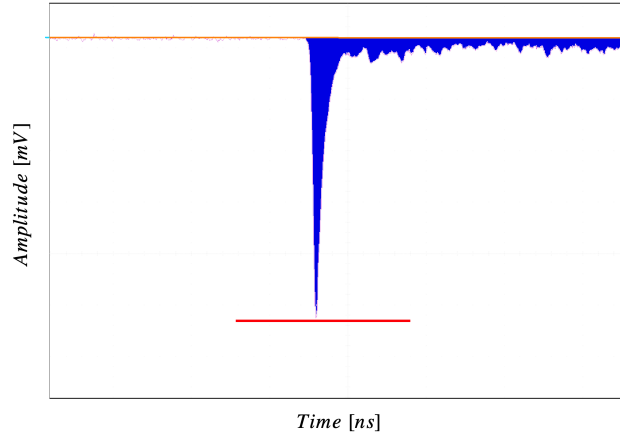


Figure 4.9: Exemplary spectra of signal acquired by one of the detectors. The pedestal of a signal is marked by an orange line. The amplitude (marked by a red line) is calculated as a lowest point of the spectrum (minimal value of the signal), the area of the signal (in blue) is proportional to the charge.

The area of the signal gives as information about the charge, which conveys information about energy deposited by gamma quanta. The charge is calculated with:

$$Q = \sum_{i=1}^n \frac{U(t_i)\Delta t}{R}, \quad (4.2)$$

where $U(t_i)$ is voltage at a time stamp i , Δt is time interval and R is constant value of resistance of given channel on DRS4 evaluation board, equal to 50Ω .

The time of the signal at given threshold is calculated on a signal spectra as intersection point between 10% of signal amplitude and the line constructed by connecting the value of signal at 30 % and 80% amplitude at leading edge of the signal.

The time difference is calculated for the signals registered in the time window set to 110 ns. The equation for calculating the time difference is:

$$\Delta T = T_{511keV} - T_{1274keV}, \quad (4.3)$$

where T_{511keV} and $T_{1274keV}$ are times at given thresholds registered for annihilation and deexcitation gamma quanta as described above as previously denoted in section 3.3. The compilation of registered time differences create a lifetime spectra.

4.3.5 Data preselection

At the beginning of every measurement day the charge spectra from both detectors was acquired in a calibration measurement. The calibration measurement inspects for differences in photomultipliers gain to ensure that the charge registered by both of detectors is consistent. For this type of measurement the thresholds are not applied and both detectors register full energy spectrum of the radioactive source. The example of such spectrum is presented in Figure 4.10. Visible in the picture are the cuts for the energies applied for the data preselection. The cuts were set to 2 pC to 5 pC for the detector gathering data about annihilation gamma quanta and from 6 pC do 10 pC for the detector gathering data about deexcitation gamma quanta.

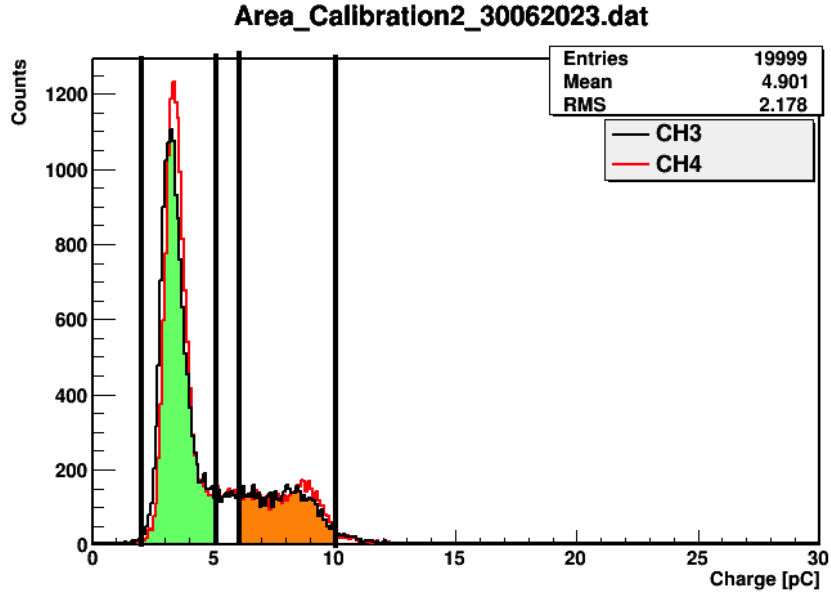


Figure 4.10: ^{22}Na isotope energy spectra registered by both PALS detectors. In region around 3.5 pC there is visible photopeak from the annihilation gamma quanta and in region of 8.5 pC there is a photopeak coming from deexcitation gamma quanta. Marked with green is the energy cut for signal from annihilation and marked in orange is the region taken for analysis of deexcitation gamma quanta.

The next step of analysis was done using PALS Avalanche program, based on iterative algorithm that fits the function to the lifetime spectra [91] and will be described in chapter section 5.1.

4.4 Measurements with J-PET scanner

4.4.1 Experimental setup

Figure 4.11 presents a picture of the modular J-PET detector. The modular detector is the most recent scanner developed by the J-PET collaboration. The previous prototype was shown to possess the capacity to be used as positronium imaging PET scanner in the experiment with cardiac myxoma and adipose tissue [3]. Most recently, the modular J-PET scanner was used to obtain a first positronium image of human brain in vivo [15]. The modular detector consists of 24 modules placed to form a cylinder. The modules can be separated for the purpose of the transportation, repair or, in case of hospital measurements, to facilitate means of quick installation around the patient. Each module contains thirteen $500 \times 6 \times 24 \text{ mm}^3$ plastic scintillation strips. The plastic scintillators chosen for the construction of modular detector were BC-404 produced by Saint-Gobain Crystals and Eljen Technology. They are characterized by good timing properties [83]. The scintillator strips are tightly wrapped in 3-M Vikuiti Enhanced Specular Reflector foil to improve light propagation and DuPont B Kapton foils to prevent loss of internally produced photons and to provide protection against external light exposure [75]. Fixed to both ends of each module are Hamamatsu MPPC-1X4CH-ARRAY S13361-6674 silicon photomultipliers (SiPMs) operating in Geiger mode, configured in a 1×4 matrix - for each scintillator strip there is 4 diodes ($6 \times 6 \text{ mm}^2$) connected optically by using Saint Gobain

BC-600 Optical Cement on both ends of the scintillator strip. Analog signal from each SiPM is sampled at two thresholds: -30 mV and -70 mV. Within gamma quanta passing those thresholds the two timestamps are registered at the leading edge and two at the trailing edge of the signal. The timestamps are recorded in continuous mode by the Data Acquisition System (DAQ).

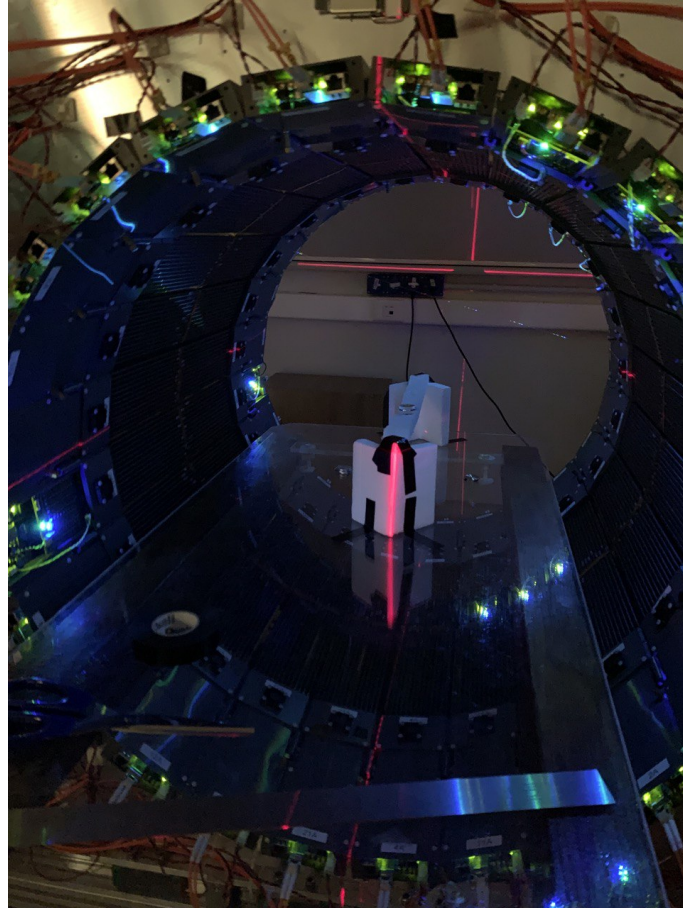


Figure 4.11: Modular J-PET detector consists of 24 modules, each of the modules consists of 13 plastic scintillators. There are 4 silicon photomultipliers (SiPMs) attached to each scintillator end.

Photomultipliers are connected with FTAB board with set of filters and Field-Programmable Gate Array (FPGA)-based Multi-Voltage Threshold (MVT) system. Data Acquisition System is probing the analog signal in the voltage domain with FPGA electronics that employ Time-to-Digital (TDC) conversion. Time when the analog signal passes the given thresholds is saved in the digitised form that allows for reconstruction of the starting time and width of the signal. Data from FTAB boards are passed to the Concentrators from which they are sent and saved on the dedicated server. More details are available in [92].

4.4.2 Measurements

During the measurement the disks were placed inside the scanner and the sources were sandwiched in between two disks of the same material. The disks were positioned in XY plane of the detector, in the center of the Z axis. The arrangements of disks and sources is

presented in the Figure 4.12. The sources used in this measurement were four sodium-22 sources shown in the Figure 4.4, with activities presented in Table 4.2.

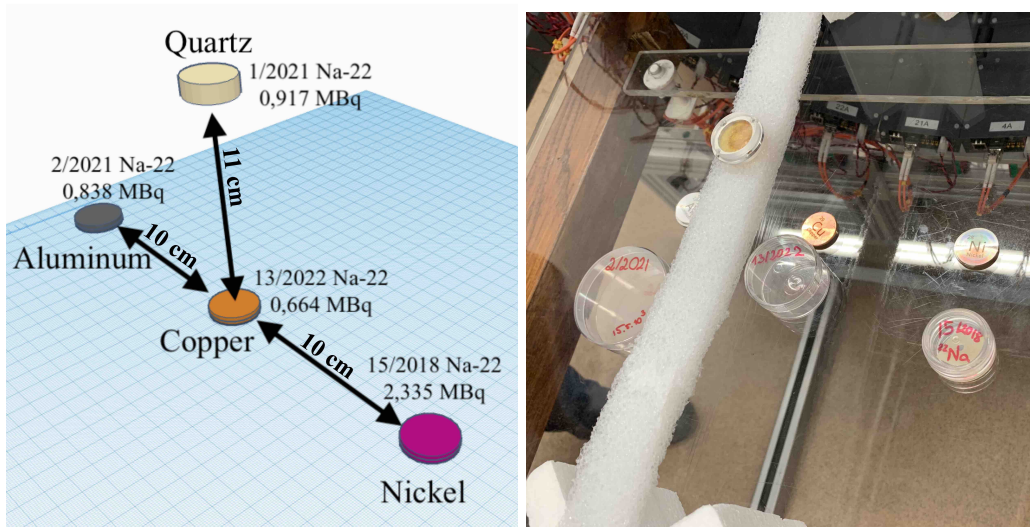


Figure 4.12: *Left*: Placement of the disks inside the J-PET scanner with respective sources and their activities. *Right*: Pictures of the disks relative placement.

The distance between the disks of aluminum, copper and nickel was 10 cm, while quartz disk was placed on a bridge 11 cm above the copper disk. This can be seen on the pictures in Figure 4.13. During the measurements the bridge has dropped gradually, so that at the end of the measurements the quartz disk was 6 cm above the copper disk.



Figure 4.13: Placement of disks inside the J-PET modular scanner. *Left*: Before the start of the measurement. *Right*: The position of quartz in the y axis had changed during the measurement.

4.4.3 Data preselection

The data was analysed using dedicated software: J-PET Framework developed by J-PET Collaboration [93]. This software allows for step by step hierarchical analysis and can be modified as needed allowing for activating and deactivating specific modules. For the means of this study an additional module was added that allowed for exporting the mean lifetime spectra from the data.

The J-PET Framework software is written in C++ programming languages and uses ROOT libraries [93, 94]. The raw data from the DAQ system is decoded into ROOT files. After that the data may undergo low-level reconstruction in which the software builds structures that resemble physical qualities of the measurement in a bottom-up manner: firstly creating time windows containing registered data, then reconstructing signals registered by photomultipliers and creating hits, which are representation on photon interactions with the scintillators.

Higher-level analysis consisted of finding events, that, in case of this study, contained three hits: two from annihilation photons and one from deexcitation photon within the time window of 10 ns, which together constitute an event with multiplicity 3. The number of qualified events with chosen multiplicity was $1.889127 \cdot 10^7$ (almost 20 million).

For the next steps of analysis a region inside the scanner was chosen that contained all four of the samples. This cut restricted data to the cylinder centred at Z axis with with 20 cm radius in XY plane and 50 cm length (in Z plane), where position 0,0,0 was set as the center of the scanner. In the Figure 4.14 the areas with the higher uptake can be seen. They correspond to the placement of the four sodium sources present on the detector at the time of the measurement. Due to arrangement of the sources 1/2021 and 13/2022 at the center of Y axis in the upper graph only three sources of activity can be distinguished.

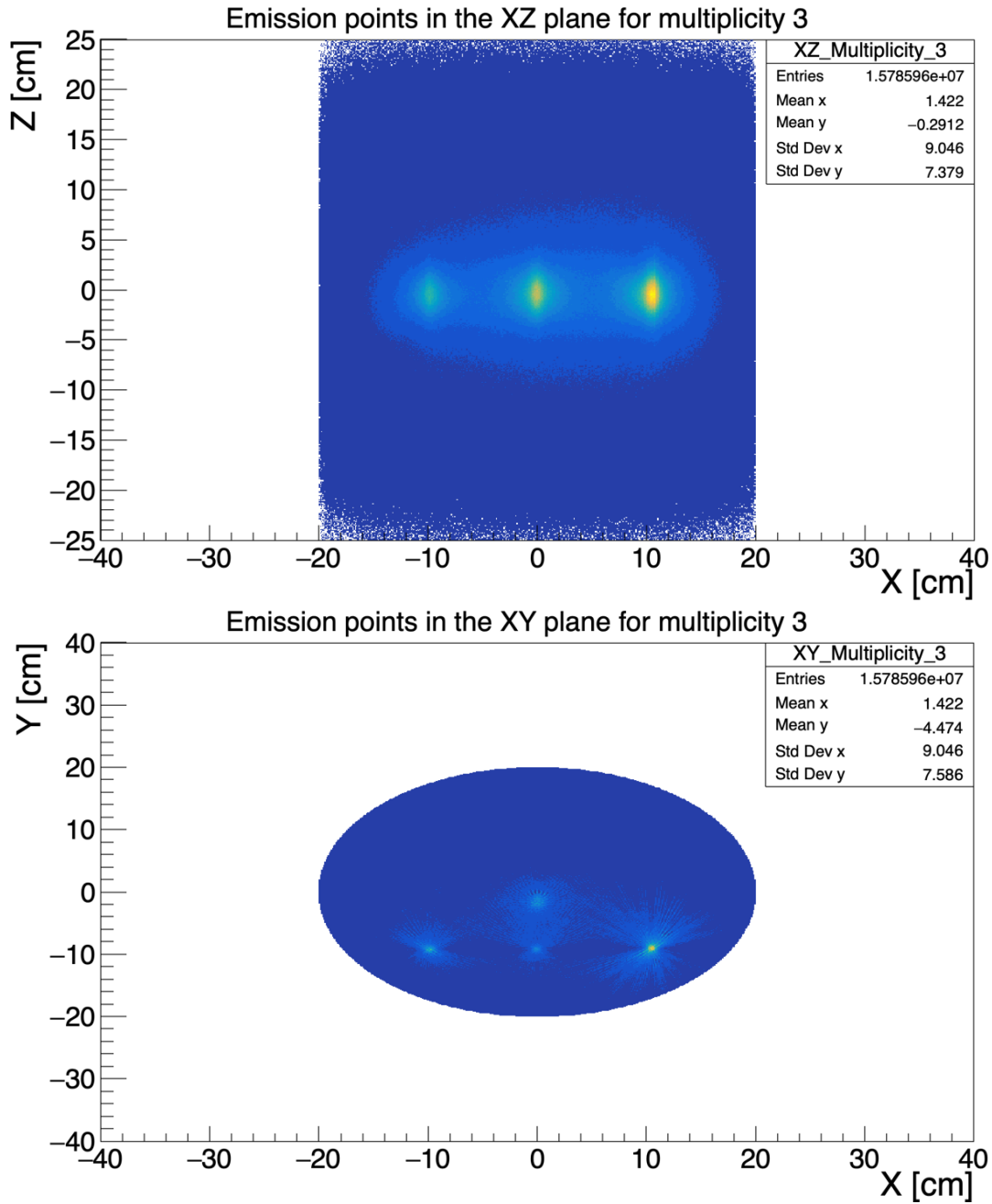


Figure 4.14: Selected regions of interest for the experiment. *Top*: The emission points in XZ plane. There are three activity regions visible as two middle sources are placed in one line on the Y axis. *Bottom*: The emission points visible in XY plane. The region of interest has radius of 20 cm. There are four visible origins of emission corresponding to the placement of the sources and samples inside the detector.

As the next step the time differences were calculated as a difference between time of emission of deexcitation photon, called the prompt photon and annihilation photons. To calculate the time difference the events with multiplicity 3 were checked for the Time Over Threshold (TOT) values of its components. The Time Over Threshold technique is applied to estimate a charge of the signal based on the signal width at specific thresholds, in case of modular J-PET those thresholds are -30 mV and -70 mV. The TOT distribution,

presented in Figure 4.15, is calculated as a mean of the TOT values registered for the signal at all photomultipliers. The TOT value for the prompt, had to be over $5 \text{ ns} \cdot V$ and for the annihilation gamma quanta, which mark the end of positronium lifetime, had to be between 2 and $5 \text{ ns} \cdot V$. In one event there had to be two annihilation photons and one prompt photon.

The times of registration of gamma quanta that fulfil the conditions above were in the next step corrected for their time of flight. The relation is applied to calculate the time of emission:

$$T_{\text{emission}} = T_{\text{hit}} - d/c, \quad (4.4)$$

where T_{hit} is the time of the hit (the moment of interaction with the scintillator), d is the distance between interaction and emission points determined for two annihilation gamma quanta with the Time Of Flight method and c is the velocity of light. The time of annihilation was calculated as the mean of time of emission of both annihilation photons. In the end the calculated time difference was:

$$\Delta T = T_{\text{stop}} - T_{\text{start}} \quad (4.5)$$

where T_{stop} is the time of annihilation and T_{start} is the time of emission of prompt photon.

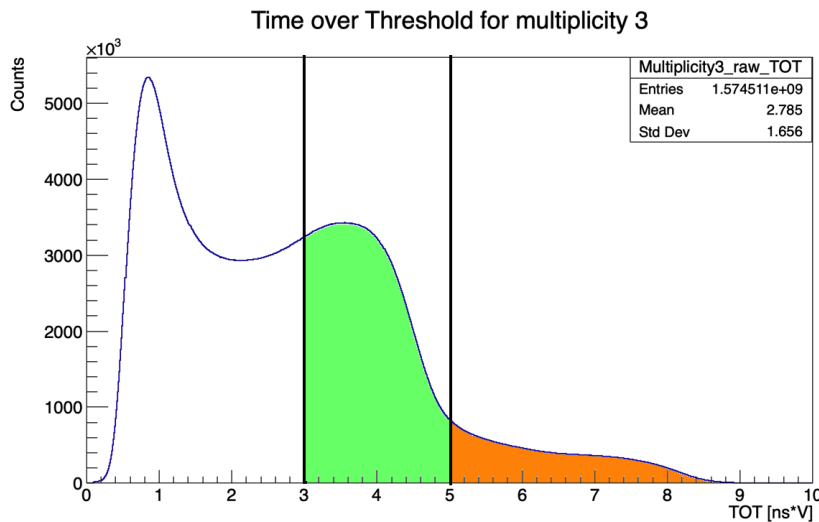


Figure 4.15: Distribution of TOT used for photon identification with Compton edges for annihilation and prompt gamma quanta from ^{22}Ne deexcitation. The green colour indicates the range chosen for selecting the annihilation photons, orange colour indicates range chosen for deexcitation photons.

The final step of framework analysis was exporting the lifetime spectra for individual samples. The list of time differences between all qualified photons was exported for further net lifetime analysis. For the samples in the bottom row the chosen regions of interests were cuboids with square base in XY plane with side lengths of 4 cm and walls in XZ plane of 8 cm. To accommodate for the sliding of the upper source in Y axis (11 cm above the table in the beginning of the measurement to 6 cm at the end) the rectangular $4 \times 8.7 \text{ cm}^2$ base was chosen in XY plane for creating the lifetime spectra. The cuts applied for the extraction of the lifetime spectra are described in Table 4.5.

Table 4.5: Positions and cut ranges from the source center position in X, Y and Z axis of modular detector for each sample. Marked with * is the mean position of the 1/2021 source in Y axis during the measurement. The starting position of this source was 1.5 cm and ending position was -3.2 cm. Due to the movement the shift for the source in Y is set to 4.35 cm instead of 2 cm.

Source name	Disk material	Placement	Axis	Position [cm]	Cut range [cm]
2/2021	Aluminum	Left	X	-10	± 2
			Y	-9	± 2
			Z	0	± 4
13/2022	Copper	Bottom center	X	0	± 2
			Y	-9	± 2
			Z	0	± 4
15/2018	Nickel	Right	X	10	± 2
			Y	-9	± 2
			Z	0	± 4
1/2021	Quartz	Upper center	X	0	± 2
			Y	-0.85*	± 4.35
			Z	0	± 4

After acquiring the spectra for all samples materials program PALS Avalanche was used to analyse the components of the lifetime spectra. Data analysis is described in subsequent chapter.

4.5 Measurements with Biograph Vision Quadra

4.5.1 Scanner characteristics

Biograph Vision Quadra PET/CT scanner that was used in course of this study is stationed at Instelhospital in Bern, Switzerland and produced by Siemens Helthineers [24]. This scanner consists of 32 crystal detector rings providing axial field of view of 106 cm. Each ring has width of 3.2 cm and consists of 38 detector blocks of 10x20 lutetium-oxorthosilicate crystals (LSO). Two adjacent detector blocks share a common electronic unit. The LSO crystals are radially organised and have dimensions of 3.2x3.2x20 mm^3 and are connected to SiPMs in a 5x5 matrix. The LSO crystals are directly coupled to an SiPM array with 16 output channels [25].

4.5.2 Measurements methodology

The measurements were performed on 27.02.2023 at Inselhospital Bern in Switzerland. During the measurements the sample disks were fixed with an adhesive tape above the examination bed in the distance of 10 cm from each other as presented in Figure 4.16. After administering ^{68}Ga solution with activity of about 5 MBq per drop to the top surface of the disks they were covered with another disk of the pair and secured with another layer of tape. The measurement lasted for one hour.

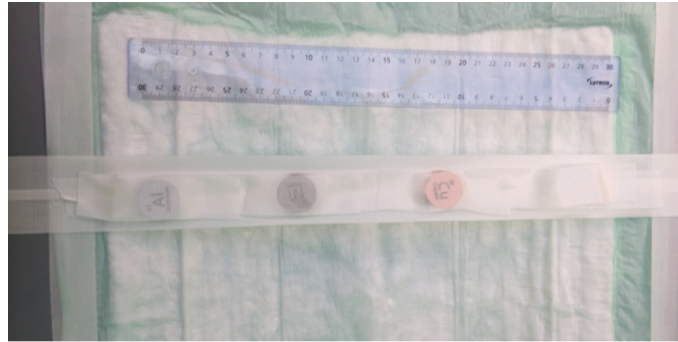


Figure 4.16: Placement of the disks in for the experiment with Biograph Vision Quadra in Inselhospital in Bern, Switzerland. The disks are fixed with adhesive tape 10 cm apart.

4.5.3 Data preselection

The data from this measurement was preselected by doctor William Steinberger. Within the coincidence window different combinations of three hits would be chosen to later be assessed for an event, which consisted of one deexcitation quantum and two annihilation quanta, by checking if they fall within a specified energy windows, as described in [10].

The data was send for lifetime analysis in the form of a histogram of lifetime differences, where first column corresponded to the number of counts and second column corresponded to the time difference in nanoseconds. The lifetime difference data were analysed using the PALS Avalanche program described in subsequent chapter section 5.1.

5. Analysis

5.1 PALS Avalanche

The program that was used in the final steps of the analysis of the data from measurements done with three systems was PALS Avalanche [91]. This software is written in C++ and uses root libraries.

The parameters of the fitted function describe the components corresponding to the mean lifetimes of positronium (or positron annihilation) that can be found for the measured sample.

The fitted function can be described as:

$$F(t) = y_0 + Area \sum_{i=0}^N \sum_{j=0}^M P_i R_j (exp(\tau_i) * Gauss(t_0^{(j)}, \sigma_j))(t), \quad (5.1)$$

where:

$$\begin{aligned} (exp(\tau_i) * Gauss(t_0^{(j)}, \sigma_j))(t) = & \frac{1}{2\tau} exp\left(\frac{\sigma^2}{2\tau^2} - \frac{t - t_0}{\tau}\right) \\ & \left(erf\left(\frac{t - t_0 - \frac{\sigma^2}{\tau}}{\sqrt{2}\sigma}\right) - erf\left(\frac{-t_0 - \frac{\sigma^2}{\tau}}{\sqrt{2}\sigma}\right) \right) \end{aligned} \quad (5.2)$$

where y_0 - background level, P_i -intensity of lifetime, α_j - fraction of given Gauss distribution, t_0 - time offset of the detector, σ - resolution of the apparatus, t - time difference between the detectors, τ - mean positron lifetime. The sum of all intensities should be given by $\sum_i^n P_i = 1$ and $\sum_j^{n_{Gauss}} \alpha_j = 1$ [90]. erf is an error function defined as:

$$erf(x) = \frac{2}{\sqrt{\pi}} \int_0^x e^{-t^2} dt. \quad (5.3)$$

The ideal spectrum would only consist of sum of exponentially decreasing determinants, which are dependent on rate of positron decay in the sample, but the shape of the function is also dependent on the timing resolution of the measurement setup, which in case of presented studies is a gaussian function. As it is visible in equation 5.1 the output function is a convolution of gaussian and exponential expressions. The parameters that are fitted in the analysis are lifetime values, which have an impact on angle of the slope, and their intensities, which tell us how much a certain component contributes to the shape of the slope, as well as the σ value, which is dependent on the resolution of the apparatus.

5.2 Fitting configuration

The configuration file is essential for the fitting procedure. In that file the user can set, among others, initial values of fit components and their type. The component types refer to the ways in which the program will apply them in the fitting procedure. The component types are as follows:

- fixed - this component is a constant, does not change in between iterations,

- lifetime fixed - this component's initial lifetime value is a constant. It does not change between iterations, but the value of intensity can freely change between the iterations,
- partially free - this component lifetime can change from the initial value within specified range. For example: the number of iterations for the fit was set to 3 and the maximal change in each iteration is 10 % of initial value in that iteration. Intensity of that component is free,
- not fixed - this component's initial value can change without constraints between iterations.

After the fitting the program generates the fitted spectra image, as shown in Figure 5.1. The result of the fitting is presented in Table 5.1. In course of this thesis, for the purpose of describing the results, the components mean lifetime values will be indicated by:

- τ_{Al} - mean lifetime value of positrons annihilating in aluminum sample,
- τ_{Ni} - mean lifetime value of positrons annihilating in nickel sample,
- τ_{Cu} - mean lifetime value of positrons annihilating in copper sample,
- τ_{p-Ps} - mean lifetime value of para-positronium,
- τ_k - mean lifetime value of positrons annihilating in kapton foil,
- τ_{direct} - other or joined components of direct positron annihilation,
- τ_{o-Ps} - mean lifetime value of ortho-positronium annihilating in quartz glass,
- τ_{pf} - mean lifetime value of ortho-positronium annihilating in Parafilm,
- τ_{add} - additional component for fitting spectra from Biograph Vision Quadra scanner.

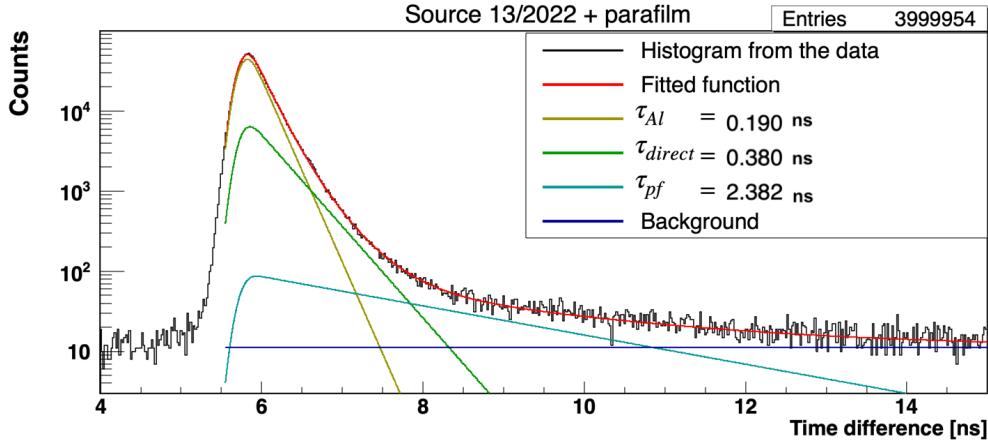


Figure 5.1: An example of fitted spectrum. The spectrum is from a measurement with source 13/2022 with newly affixed layer of Parafilm between two aluminum disks. On the horizontal axis is the time difference between the registration of deexcitation and annihilation gamma quanta. On the vertical axis is the number of counts. The red line indicates the fitted function, the yellow line corresponds to the positron mean lifetime of the component of positron direct annihilation in aluminium sample disk τ_{Al} , while the green line - of the direct annihilation of positrons in kapton and parafilm τ_{direct} , the blue line - of the ortho-positronium annihilation in parafilm τ_{pf} . The dark blue line marks the background level that is calculated here as a mean value of 50 bins on the left side of the spectrum. Fitted parameter of detector resolution $\sigma = 0.09949(20)$ is described in equation (5.2).

Table 5.1: An exemplary table of fit results for the measurement of a metal disk with source 13/2022 that was done in search of the lifetime values τ_{direct} and τ_{pf} . The τ_{Al} corresponds to positron mean lifetime in aluminum sample. The value of $\chi^2/dof = 1.76$. Fitted parameter of detector resolution $\sigma = 0.09949(20)$ is described in equation (5.2). The uncertainties are indicated in brackets, the values that are constant in the fitting process (fixed) are presented without the uncertainties. As mentioned in section section 5.1 the sum of intensities of the fit components should be equal to one.

Component	Lifetime [ns]	Intensity
(τ_{Al}, i_{Al})	0.19	0.84643(98)
$(\tau_{direct}, i_{direct})$	0.3799(14)	0.18128(86)
(τ_{pf}, i_{pf})	2.382(51)	0.01076(20)

5.3 Determining the parameters for kapton and parafilm

The sodium sources used in the measurements, described in detail section 4.2, are encapsulated in layers that protect them from damage and leaking. During positron passing through them, annihilation might occur. Due to small size of the sample it is not possible to spatially separate annihilations in mentioned layers from ones in the tested sample. To ensure precision in determining the studied sample contribution to the spectrum the

values of lifetime and intensity of the protective layer components must be assessed prior to the main measurement. Described below are the steps of the procedure applied by the author in order to determine those components is the measurement with a source of known constant parameters of the fit. The first step being measurement with source of known constant parameters of the fit and the second step the measurement with the new source and a sample with known value of positron mean lifetime.

In order to establish the value of the protective layers' components for the new source 13/2022 the author applied the approach of finding the value of positron mean lifetime for an aluminum sample with the use of source 2/2021 of known constant parameters of the fit. The source 2/2021 was previously used by the author and other researchers in the lab and its values of fit parameters that correspond to kapton foil and Parafilm were established prior to this study [8]. As a next step the author had performed a measurement with new 13/2022 source and the same sample with established positron mean lifetime value. In this way the aluminum sample spectra can be separated from the data corresponding to the source's protective layers.

Presented in the Figure 5.2 is the result of fitting of the spectrum of the source 2/2021 with aluminum disks. Those disks are not a research object of this thesis and serve only the purpose of establishing the values of the components. Results of the fit are presented in Table 5.2 and Figure 5.2. Based on those fit results the value of mean lifetime of component corresponding to positron annihilation in this disk was set as 190 ps (lifetime fixed component) in the subsequent measurements.

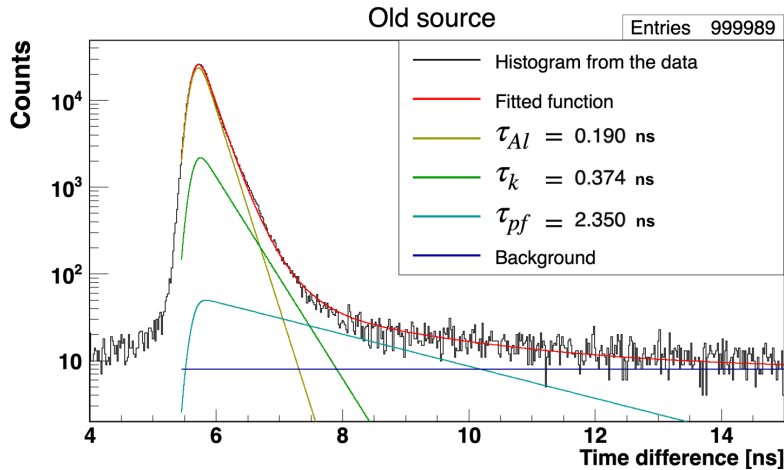


Figure 5.2: The spectrum of the 2/2021 source encapsulated in kapton and Parafilm layers fastened between two aluminum disks. The fit was done in search for the mean lifetime τ_{Al} of the component indicated here with a yellow line. The red line corresponds to the fitted spectra, the green line corresponds to the positron annihilation in kapton foil, the blue line corresponds to the ortho-positronium annihilation in Parafilm and the dark blue line indicates the background level. The value of $\chi^2/dof = 2.04$. Fitted parameter of detector resolution $\sigma = 0.10042(28)$.

Table 5.2: Results of fitting the spectra for source 2/2021 with aluminum disk (different from the thesis main study aluminum sample). The value of $\chi^2/dof = 2.04$. Fitted parameter of detector resolution $\sigma = 0.10042(28)$. The uncertainties are indicated in brackets, the values that are constant in the fitting process (fixed) are presented without the uncertainties.

Component	Lifetime [ns]	Intensity
(τ_{Al}, i_{Al})	0.18980(37)	0.7413(11)
(τ_k, i_k)	0.374	0.1
(τ_{pf}, i_{pf})	2.35	0.01

The 13/2022 source purchased by the Jagiellonian University was initially set in kapton foil. The source was later encapsulated in additional protective layer of Parafilm [95]. Parafilm is a flexible, self-sealing, water resistant film, that can be stretched and affixed to the kapton foil to protect the source from leakage in contact with biological samples. Most of the sources available in the PALS laboratory at the Jagiellonian University are secured with Parafilm as they are used for the purposes of biological studies. After the addition of Parafilm layer the new source was measured with PALS.

The obtained data, from the measurement with new source encapsulated in kapton film and Parafilm, were analysed with PALS Avalanche software with initial values of parameters presented in Table 5.3. The results of this fit are presented in Table 5.1 and Figure 5.1.

Table 5.3: The initial parameters for the fit of spectra of source 13/2022 encapsulated in protective layers. The partially free components can vary up to 10 % of initial value per each iteration. The value of intensity of lifetime fixed component can change freely. As mentioned in section section 5.1 the sum of intensities of the fit components should be equal to one.

Component	Lifetime value [ns]	Intensity value	Type
(τ_{Al}, i_{Al})	0.19	0.89	lifetime fixed
$(\tau_{direct}, i_{direct})$	0.374	0.1	partially free
(τ_{pf}, i_{pf})	2.35	0.01	partially free

As it can be seen in Figure 5.1, the newfound value for the τ_{direct} is equal to 0.38 ns and has an intensity of 18%. This intensity is higher than expected of annihilation in kapton alone. Based on the literature it was assumed that the lifetime of positron in kapton foil is equal to 0.374 ns, and the amount of the positrons that annihilate in it is about 10% of the all annihilations registered by the PALS [26, 96]. In this case the component with mean lifetime value of τ_{direct} may be a combination of the components from direct annihilation in kapton foil and direct annihilation in Parafilm. The modified initial parameters of the fit are presented in Figure 5.4. After assuming the fixed constant of kapton foil as 0.374 ns and repeating the fitting procedure, the additional component of direct annihilation of positrons in parafilm is found to be 0.385 ps with intensity 8% as presented in Figure 5.3. This results are summarised in Table 5.5. The results presented here served to establish the constant values in the fitting of the spectra measured with source 13/2022.

Table 5.4: The new initial parameters for the fit of spectra of source 13/2022 encapsulated in protective layers. The added parameter with the mean lifetime τ_k was chosen based on literature [26, 96]. The partially free components can 10 % of initial value in each of 3 iterations. The value of intensity of lifetime fixed component can change freely.

Component	Lifetime value [ns]	Intensity value	Type
(τ_{Al}, i_{Al})	0.19	0.81	lifetime fixed
(τ_k, i_k)	0.374	0.1	fixed
$(\tau_{direct}, i_{direct})$	0.38	0.08	partially free
(τ_{pf}, i_{pf})	2.4	0.01	partially free

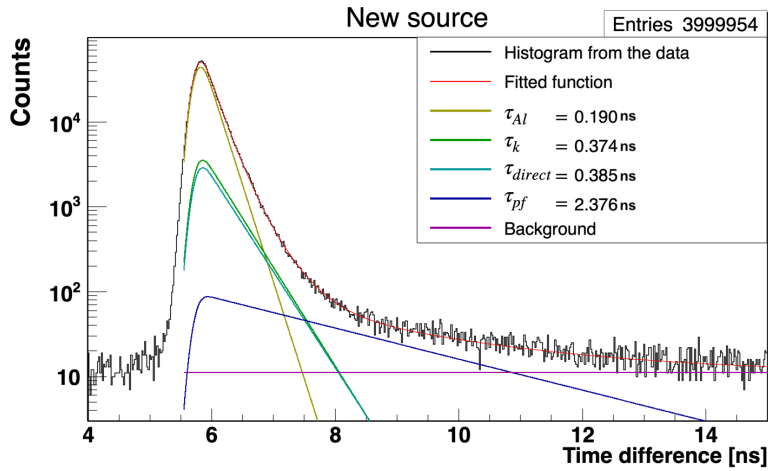


Figure 5.3: The spectrum of the 13/2022 source encapsulated in kapton and Parafilm layers fastened between two aluminum disks. The red line indicates the fitted spectra, the yellow line corresponds to the positron annihilation in aluminum disks, the green line corresponds to the positron annihilation in kapton foil, the blue line corresponds to the direct positron annihilation in Parafilm, the dark blue line corresponds to the ortho-positronium annihilation in Parafilm and the purple line indicates the background level. The value of $\chi^2/dof = 1.76$. Fitted parameter of detector resolution $\sigma = 0.09947(20)$

Table 5.5: Results of fitting the spectra for source 13/2022 with aluminum disk (different than sample used in the study) to find the constant values for kapton and Parafilm layers in spectra fitting. In this fit there is additional constant of 0.374 ns with intensity of 10% corresponding to positron lifetime in kapton [26, 96]. The value of $\chi^2/dof = 1.76$. Fitted parameter of detector resolution $\sigma = 0.09947(20)$

Component	Lifetime [ns]	Intensity
(τ_{Al}, i_{Al})	0.19	0.85
(τ_k, i_k)	0.374	0.1
$(\tau_{direct}, i_{direct})$	0.385(30)	0.08307(86)
(τ_{pf}, i_{pf})	2.376(51)	0.01086(20)

5.4 Analysis of data from PALS

The spectra from PALS measurements were fitted using previously established values described in section 5.3 presented in Table 5.6 as constants.

Table 5.6: The initial values of parameters in the PALS spectra fitting. (τ_{Al}, i_{Al}) , (τ_{Ni}, i_{Ni}) and (τ_{Cu}, i_{Cu}) are components corresponding to positron annihilation in metal, (τ_k, i_k) is positron annihilation in kapton, $(\tau_{direct}, i_{direct})$ is direct positron annihilation in Parafilm and (τ_{pf}, i_{pf}) is ortho-positronium annihilation in Parafilm.

Component	Lifetime [ns]	Intensity	Type
(τ_{Al}, i_{Al})	≈ 0.18	0.81	partially free
(τ_{Ni}, i_{Ni})	≈ 0.17		
(τ_{Cu}, i_{Cu})	≈ 0.15		
(τ_k, i_k)	0.374	0.1	fixed
$(\tau_{direct}, i_{direct})$	0.385	0.08	fixed
(τ_{pf}, i_{pf})	2.4	0.01	fixed

The sum of the i_k, i_{direct} and i_{pf} intensities in Table 5.6 is equal to 19%. That is equal to the percent of the positrons that annihilate in the source's protective layers. The rest of the positrons, which pass through those layers may annihilate fully inside the sample, depending on the density of the measured material. The average and maximum positron path length is described in section 3.8. The thickness of the aluminum, copper, nickel and quartz disks used in this study disallows for most of the positrons emitted from the ^{22}Na source to permeate outside the sample.

For fitting the spectra from metal samples measurements (nickel, copper and aluminum disks) there is one partially free parameter in addition to the constants presented in Table 5.6: that component corresponds to the direct annihilation of positrons in the disk.

As noticeable in Table 5.2, in case of fitting only one free component, the final values of the intensities do not sum up to 100%. As the positrons that pass through kapton and Parafilm layers annihilate entirely in the metal sample, the value of intensity of the τ_{Al} , τ_{Cu} and τ_{Ni} component each should equate to 81%. This value of intensity is assumed in the final results. The uncertainty of that intensity value was calculated as a sum of the

uncertainties of intensities established previously: for Parafilm and kapton. Based on that approach, the value of uncertainty is established as 0.11%.

In case of quartz glass disk data there are three additional components present in the spectra fit. The initial parameters of the quartz glass spectra fit are presented in Table 5.7.

Table 5.7: The initial values of parameters in the quartz glass spectra fitting of data from PALS measurement. (τ_{p-Ps}, i_{p-Ps}) is component corresponding to para-positronium annihilation [35], (τ_k, i_k) is positron annihilation in kapton, $(\tau_{direct1}, i_{direct1})$ is direct positron annihilation in Parafilm, $(\tau_{direct2}, i_{direct2})$ is direct positron annihilation in quartz glass, (τ_{o-Ps}, i_{o-Ps}) is ortho-positronium annihilation in quartz glass and (τ_{pf}, i_{pf}) is ortho-positronium annihilation in Parafilm.

Component	Lifetime [ns]	Intensity	Type
(τ_{p-Ps}, i_{p-Ps})	0.125	0.3	lifetime fixed
(τ_k, i_k)	0.374	0.1	fixed
$(\tau_{direct1}, i_{direct1})$	0.385	0.08	fixed
$(\tau_{direct2}, i_{direct2})$	≈ 0.4	0.1	partially free
(τ_{o-Ps}, i_{o-Ps})	≈ 1.5	0.5	partially free
(τ_{pf}, i_{pf})	2.4	0.01	fixed

5.5 Analysis of data from modular J-PET scanner

Due to the time difference resolution of the J-PET scanner, estimated to 520 ps (FWHM), the components corresponding to direct annihilation of positrons in kapton foil and parafilm (in case of quartz glass disk also the para-positronium annihilation) were considered as a single component [15].

The fit for the copper and aluminium samples comprised of three components, which are delineated in Table 5.8. The fit for nickel disks comprised of two components delineated in Table 5.9. The fitting program did not found a third component in an alternative fit with three components. The reason for difference in spectra composition of the nickel disks is most likely caused by the difference in 5/2019 source, which, unlike the rest of the sodium sources, wasn't covered in Parafilm and had smaller radius of the kapton foil. In case of the quartz glass sample the fit comprised of two components described in Table 5.10.

Table 5.8: Initial parameters of the fit components for the aluminum and copper disks measurements in Modular J-PET scanner. $(\tau_{direct}, i_{direct})$ is the joined component for direct annihilation in kapton and parafilm, (τ_{Al}, i_{Al}) and (τ_{Cu}, i_{Cu}) are the components corresponding the direct annihilation in aluminum and copper. (τ_{pf}, i_{pf}) is the ortho-positronium annihilation in parafilm. All components' intensities are free so they were not included in this table.

Component	Initial lifetime value [ns]	Type
$(\tau_{direct}, i_{direct})$	≈ 0.4	partially free
(τ_{Al}, i_{Al}) or (τ_{Cu}, i_{Cu})	≈ 0.18 ≈ 0.16	partially free
(τ_{pf}, i_{pf})	≈ 2.4	partially free

Table 5.9: Initial lifetime values of the components of the fit for the nickel disks measurements in Modular J-PET scanner. $(\tau_{direct}, i_{direct})$ is the joined component for direct annihilation in kapton and parafilm, (τ_{Ni}, i_{Ni}) is the short component for direct annihilation in nickel. All components' intensities are free so they were not included in this table.

Component	Initial lifetime value [ns]	Type
$(\tau_{direct}, i_{direct})$	≈ 0.4	partially free
(τ_{Ni}, i_{Ni})	≈ 0.16	partially free

Table 5.10: Initial lifetime values of the components of the fit for the quartz glass disks measurements in Modular J-PET scanner. $(\tau_{direct}, i_{direct})$ is the joined component for direct annihilation and para-positronium annihilation, (τ_{o-Ps}, i_{o-Ps}) is the ortho-positronium annihilation. All components' intensities are free so they were not included in this table.

Component	Initial lifetime value [ns]	Type
$(\tau_{direct}, i_{direct})$	≈ 0.4	partially free
(τ_{o-Ps}, i_{o-Ps})	≈ 1.5	partially free

5.6 Analysis of data from Biograph Vision Quadra

The disks measurement in Biograph Vision Quadra scanner was performed with use of ^{68}Ga as a positron source. Unlike the ^{22}Na source, which due to its long half lifetime is encapsulated in protective layers, the ^{68}Ga source was applied on top of the disks as a water solution. Therefore no components coming from kapton or parafilm contribute to those spectra's shape.

It was verified that the fit with only one component does not describe the spectra shape. To fit two components it was necessary to fix at least one of the components of the spectra to obtain the lifetime values in expected range. Example of a spectrum fitted with one component is presented in Figure 5.4.

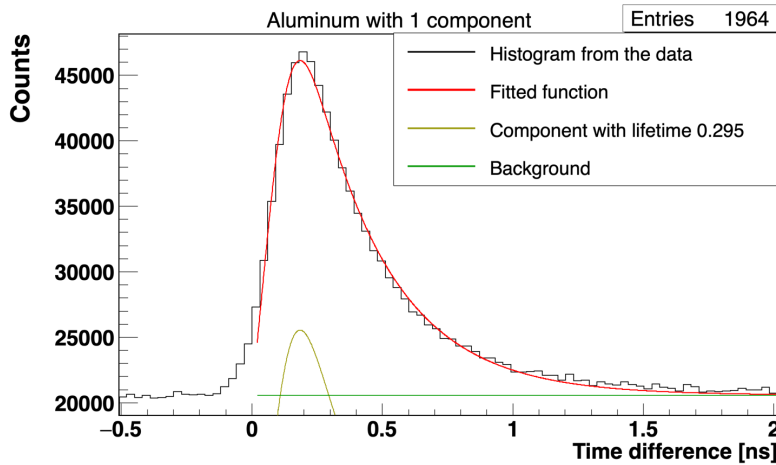


Figure 5.4: Spectra fitted with one component. The value of χ^2/dof of this fit is equal to 2.95. The red line indicates the fit, which in this case does not describe the data well.

Under the assumption that the spectra can be described by two components (from the positron annihilation in disks and one additional component) there was a fitting performed on aluminum disks spectrum in search of the value of that additional component. The additional component should be invariable between as the disks as were measured

simultaneously and prepared the in same manner.

The value of aluminum lifetime was chosen as 0.181 ns lifetime-fixed component with free to change initial value of intensity of 60%. The result of this fitting is presented in Table 5.11 and in Figure 5.5.

The value of uncertainty of that components intensity is equal to 30%, but as the intensity of remaining component is 56.18(39) % and the sum of components intensities should equate to 100% this high uncertainty was discoloured as a bug in the software, which was not solved before completion of this thesis. The value found for additional component was used as a constant in fitting of the disks. Lifetime value of that additional component was eventually set as 0.535 ns with intensity of 43%

Due to high background visible in the spectra, caused among others by ^{176}Lu decay, the spectra start from high values of counts, which had to be taken under the consideration in the fit configuration.

Table 5.11: Results of the fitting the spectra extracted for aluminum disk from measurements with Biograph Vision Quadra in a search of the additional components distinct from the positron annihilation in the disks. The goodness of the fit, measured as χ^2/dof is equal to 1.31. Fitted parameter of detector resolution $\sigma = 0.10688(51)$

Component	Lifetime [ns]	Intensity
(τ_{Al}, i_{Al})	0.181	0.5618(39)
(τ_{add}, i_{add})	0.5347(57)	0.43(31)

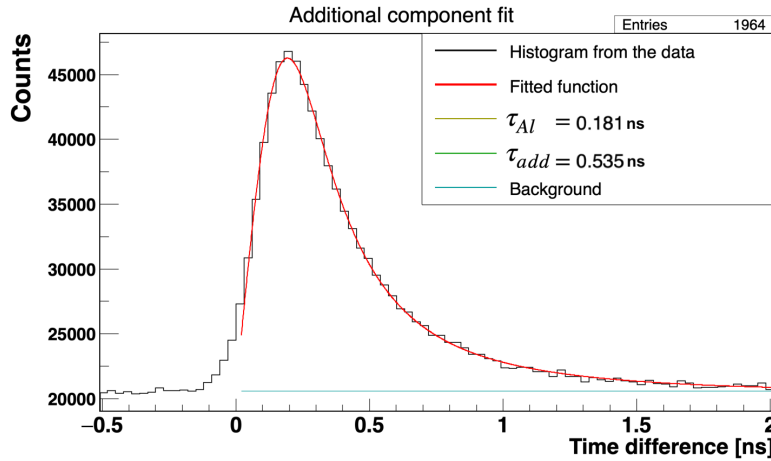


Figure 5.5: The fitted spectrum extracted for aluminum disk form measurements with Biograph Vision Quadra scanner. The fit was done in search for the value of component additional to the disk material component. The red line indicates a fitted function. Due to the high background the lines indicating components' input are shifted down.

The fit for the nickel and aluminium samples comprised of two components, which are delineated in Table 5.12. The components of fit for the copper disk are described in Table 5.13 and for quartz glass disks in Table 5.14.

Table 5.12: Initial values of the components of the fit for the aluminum and nickel disks measured in Biograph Vision Quadra scanner. (τ_{Al}, i_{Al}) is annihilation in aluminum, (τ_{Ni}, i_{Ni}) is annihilation in nickel, (τ_{add}, i_{add}) is an additional constant in the fit.

Component	Initial life-time value [ns]	Initial intensity	Type
(τ_{Al}, i_{Al})	0.181	0.57	partially free
(τ_{Ni}, i_{Ni})	0.17		
(τ_{add}, i_{add})	0.535	0.43	fixed

Table 5.13: Initial lifetime values of the components of the fit for the copper disks measured in Biograph Vision Quadra scanner. (τ_{Cu}, i_{Cu}) is annihilation in copper, (τ_{add}, i_{add}) is an additional constant in the fit.

Component	Initial life-time value [ns]	Initial intensity	Type
(τ_{Cu}, i_{Cu})	0.15	0.57	partially free
(τ_{add}, i_{add})	0.535	0.43	lifetime-fixed

Table 5.14: Initial values of the components of the fit for the quartz glass disks measured in Biograph Vision Quadra scanner. (τ_{p-Ps}, i_{p-Ps}) is para-positronium annihilation, (τ_{add}, i_{add}) is an additional constant in the fit, (τ_{o-Ps}, i_{o-Ps}) is ortho-positronium annihilation.

Component	Initial life-time value [ns]	Initial intensity	Type
(τ_{p-Ps}, i_{p-Ps})	0.125	0.2	lifetime fixed
(τ_{add}, i_{add})	0.535	0.43	fixed
(τ_{o-Ps}, i_{o-Ps})	≈ 1.5	0.3	partially free

6. Results

At the outset, this Chapter presents the results from each measurement system individually. The later part of this Chapter shows the comparison and discussion of time resolution, mean lifetimes, goodness of the fit, intensities and other factors that may have impacted the results.

6.1 PALS

The results of the fitting of the merged data from sets of measurements done with PALS technique are shown in Table 6.1. The obtained positron mean lifetime for aluminum is longer than for nickel and copper, similarly to the positron lifetime in bulk that is shorter for copper and nickel than for aluminum according to the literature [48]. As expected, longer mean lifetime of ortho-positronium was obtained for quartz glass.

Table 6.1: Values of the fitted parameters for the of time difference spectra obtained with PALS. χ^2_ν is the goodness of the fit defined as χ^2 per degrees of freedom.

Measured material	Component	Lifetime [ns]	Intensity [%]	χ^2_ν	σ
Aluminum	τ_{Al}	0.19207(16)	81.00(11)	2.64	0.10395(11)
Nickel	τ_{Ni}	0.14388(14)	81.00(11)	2.09	0.10868(11)
Copper	τ_{Cu}	0.15473(14)	81.00(11)	2.12	0.10783(11)
Quartz	τ_{o-Ps}	1.5863(15)	43.789(41)	1.98	0.11191(15)

6.2 Modular J-PET

The results of the fitting of the data from the measurement done with modular J-PET scanner are shown in Table 6.2. The obtained mean lifetime values for metal disks are, as expected, one magnitude shorter than for quartz glass. The differences between the positron lifetime values of aluminum, nickel and copper do not resemble the relation presented in literature [48], in which positron lifetime in bulk in nickel and copper are similar and lower than in aluminum.

Table 6.2: Values of the fitted parameters for the time difference spectra obtained with J-PET detector.

Measured material	Component	Lifetime [ns]	Intensity [%]	χ^2_ν	σ
Aluminum	τ_{Al}	0.1414(15)	0.4384(15)	15.16	0.27776(74)
Nickel	τ_{Ni}	0.10570(47)	0.5849(10)	5.18	0.28332(48)
Copper	τ_{Cu}	0.1637(14)	0.5257(19)	4.64	0.26857(91)
Quartz	τ_{o-Ps}	1.4331(27)	0.52575(91)	11.68	0.31755(72)

6.3 Biograph Vision Quadra

The results of the fitting of the data from the measurement done with Biograph Vision Quadra scanner are shown in Table 6.3. The relation between obtained mean lifetime values for metal disks resemble the theoretical positron lifetime in bulk portrayed in literature [48]. The values of positron mean lifetime for copper and nickel are lower than for the aluminum. As expected, the ortho-positronium mean lifetime in quartz glass is one magnitude longer than mean positron lifetime in metals.

Table 6.3: Values of the fitted parameters for the spectra of time differences obtained with Biograph Vision Quadra in Bern.

Measured material	Component	Lifetime [ns]	Intensity [%]	χ^2_ν	σ
Aluminum	τ_{Al}	0.1908(12)	0.5973(22)	1.30	0.10541(55)
Nickel	τ_{Ni}	0.1477(11)	0.5222(22)	1.26	0.10541(55)
Copper	τ_{Cu}	0.1659(12)	0.7517(32)	1.12	0.10227(65)
Quartz	τ_{o-Ps}	1.636(28)	0.863(10)	0.97	0.1261(12)

6.4 Comparison

6.4.1 Time resolution of detection setups

The mean lifetime difference spectrum is a convolution of a gaussian and exponential functions, as described in the section 5.1. The precision of determining the exponentially decreasing components depends on the time difference resolution of the detector. Comparing the normalised spectra, which can be seen in Figure 6.1, from the measurements on the three setups, one can see how the timing resolution of the setup influences the shape of the spectra. The larger gaussian smearing of the spectra from the measurement done on modular J-PET stands out from the slimmer slopes coming from the measurements done with PALS setup and Biograph Vision Quadra scanner. This may result in less precision in determining the values of positron and positronium lifetimes from the measurement done with modular J-PET.

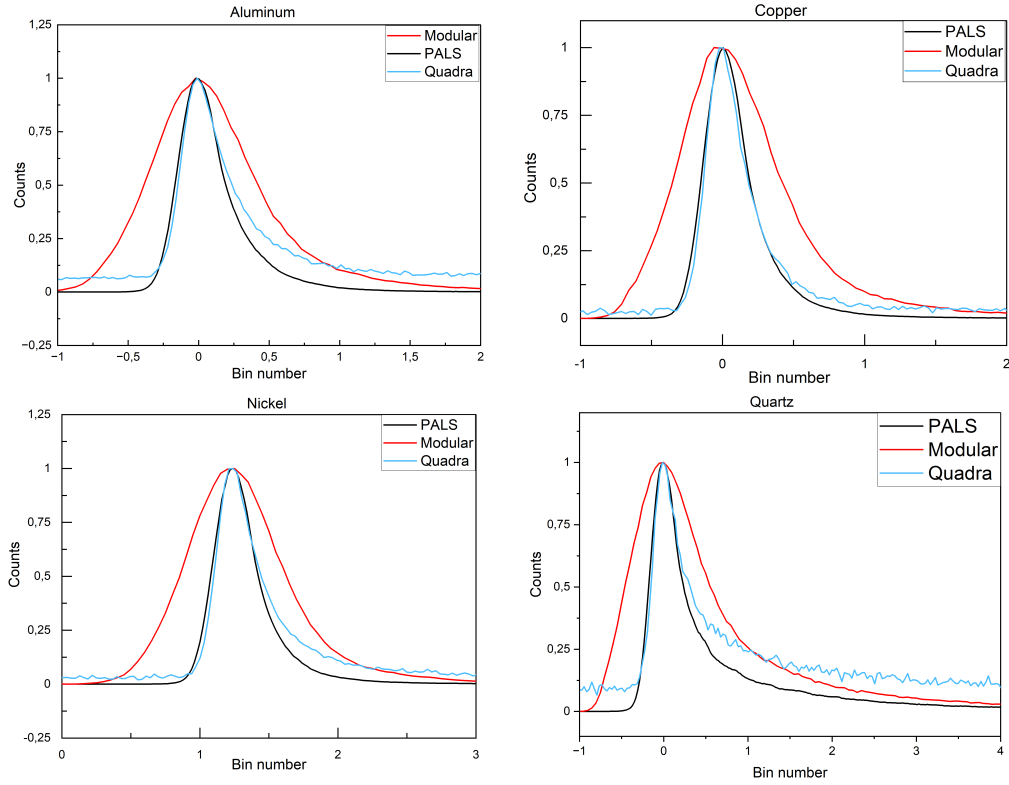


Figure 6.1: The comparison of the spectra from disks measurements on the three setups. All the spectra were normalised and shifted to overlay the spectra peaks. The red line indicates spectra from measurements with modular J-PET, the black line corresponds to the measurements done with PALS, the blue line indicates the spectra from Biograph Vision Quadra measurements. *Top row:* The left graph shows the spectra from aluminum disks measurements, the right graph shows the spectra from copper disks measurements. *Bottom row:* The left graph shows the spectra from nickel disks measurements, the right graph shows the spectra from quartz disks measurements.

In Table 6.4 the comparison of full width at half-maximum (FWHM) of the spectra resolution is presented. The FWHM value relates to the fit parameter σ and is described as:

$$FWHM = 2\sigma\sqrt{2\ln 2}. \quad (6.1)$$

The results shows that the timing difference resolution of J-PET detector on average 2.7 times worse than the PALS detector and on average 2.6 times worse than the timing resolution of Biograph Vision Quadra scanner.

Table 6.4: The value of FWHM of the fit for the spectra from PALS, modular J-PET and Biograph Vision Quadra measurements.

Sample	FWHM [ns]		
	PALS	J-PET	Quadra
Aluminum	0.24481(26)	0.6541(17)	0.2445(12)
Copper	0.25394(25)	0.6325(21)	0.2483(13)
Nickel	0.25595(26)	0.6672(11)	0.2526(16)
Quartz	0.26355(35)	0.7478(17)	0.2969(28)

During the measurement in Biograph Vision Quadra and J-PET the disks were measured simultaneously but positioned differently in the scanner. The placement of the disks in Quadra scanner was along its X axis. In the Modular J-PET scanner the sources were arranged in XY plane, perpendicular to the scanner axis. The sources placement affects the time difference resolution of the spectra, as it can be seen with the FWHM values for the spectrum from modular J-PET: the spectra for copper disks that were positioned in the center of the detector has the lowest FWHM value from this measurement.

The differences in time resolution of the PALS measurements may be the result of temperature fluctuations in the lab.

6.4.2 Mean lifetimes

The comparison of the mean lifetime values for the components of aluminum (τ_{Al}), nickel (τ_{Ni}), copper (τ_{Cu}) and quartz glass (τ_{o-Ps}) is presented in Figure 6.5.

Table 6.5: The comparison of the mean lifetime values for aluminum, nickel, copper and quartz glass from measurements with PALS, modular J-PET scanner and Biograph Vision Quadra scanner and literature. In case of aluminum τ_c is the lifetime value determined for positron annihilation in metal lattice by empirical study, τ_m is the lifetime value determined for positron trapped in monovacancy.

Disk material	PALS [ns]	J-PET [ns]	Quadra [ns]	Literature [ns]
Aluminum	0.19207(16)	0.1414(15)	0.1908(12)	$\tau_c = 0.161 \pm 2$, $\tau_m = 0.243 \pm 1$ [53]
Nickel	0.14388(14)	0.10570(47)	0.1477(11)	0.160 [51]
Copper	0.15473(14)	0.1637(14)	0.1659(12)	0.1580(15) [50]
Quartz	1.5863(15)	1.4331(27)	1.636(28)	1.538(36) [10]

The comparison of the values of mean lifetimes from measurements of the disks as a percentage difference is presented in Table 6.6. The percentage difference between the results is described by the equation below:

$$\frac{a_{max} - a_{min}}{(a_{max} + a_{min})/2} \cdot 100\%, \quad (6.2)$$

where a_{max} is the greater value and a_{min} is the lower value. It was not possible to state precisely the theoretical mean lifetime value of components to compare them with the measured results, as the mean lifetime may depend on the process of production. In turn

the PALS was considered most precise method of mean lifetime value determination in these study and it was chosen as a value of reference.

For the aluminum disks the τ_{Al} values are consistent in 30% between the PALS and modular J-PET measurements and in 0.66% between PALS and Biograph Vision Quadra measurements. For the nickel disks the τ_{Ni} values are consistent in 31% between the PALS and modular J-PET measurements and in 2.6% between PALS and Biograph Vision Quadra measurements. For the copper disks the τ_{Cu} values are consistent in 5.6% of their value between the PALS and modular J-PET measurements and in 7% of their values between PALS and Biograph Vision Quadra measurements. For the quartz glass disks the τ_{o-Ps} values are consistent in 10% between the PALS and modular J-PET and 3.1% between PALS and Biograph Vision Quadra measurements.

Table 6.6: The comparison of the values of mean lifetimes from measurements of the disks of aluminum (τ_{Al}), nickel (τ_{Ni}), copper (τ_{Cu}) and quartz glass (τ_{o-Ps}) as a percentage difference.

Mean lifetime	Percentage difference [%]	
	PALS and J-PET	PALS and Quadra
τ_{Al}	30	0.66
τ_{Ni}	31	2.6
τ_{Cu}	5.6	7.0
τ_{o-Ps}	10	3.1

The biggest differences in lifetime values between PALS and J-PET can be observed for aluminum and nickel disks which were placed 10 cm from the center of the X axis of the modular J-PET scanner. The lowest difference percent is observed for copper, which was arranged in the center of the modular J-PET detector. The placement of the disks in the scanner may play a role in accuracy of the results.

Overall the mean lifetime values obtained with PALS and Biograph Vision Quadra convey the relation presented in literature, where the positron lifetime in bulk for nickel and copper are similar and shorter than for aluminum [48]. The positron mean lifetime values obtained with modular J-PET regarding the metal samples do not exhibit this relation as the lifetime in copper was determined to be longer than in nickel and aluminum. It is worth to note though that the given samples may not convey the relation presented in literature due to the defects developed in the production process.

The results of quartz spectra analysis show that the value of ortho-positronium mean lifetime determined by PALS measurement and Biograph Vision Quadra measurement is in agreement with the literature value within two standard deviations. The result of modular J-PET measurements is in agreement with literature within three standard deviations [10].

6.4.3 Goodness of the fit

The comparison of the χ^2_ν value, shown in Table 6.7, which is the estimate of the goodness of the fit divided by the degrees of freedom, shows that values were significantly higher for the fits of the spectra from the modular J-PET detector. This may have resulted from the poorer time difference resolution of the spectra. In case of quartz glass data the worse χ^2_ν may result from the small coincidence window. The tail of the time difference distribution is cut off at 10 ns, which resulted in difficulties in background estimation.

Table 6.7: Comparison of χ^2_ν values, calculated as χ^2 per degrees of freedom, which estimate the goodness of the fits obtained from measurements with PALS system, modular J-PET scanner and Biograph Vision Quadra scanner.

Sample	χ^2_ν		
	PALS	J-PET	Quadra
Aluminum	2.6	15.2	1.3
Nickel	2.1	5.2	1.3
Copper	2.1	4.6	1.1
Quartz	2.0	11.7	0.97

6.4.4 Intensities

The intensities of disk material components have been shown to be lower in case of the measurements in the J-PET scanner than the PALS. The comparison of the intensities of the positron lifetime components are presented in Table 6.8. This observation holds also for measurements performed with the same source 13/2022 in both PALS and modular J-PET proving that this characteristic does not arise from differences in source casing. The disparity may arise from different geometrical conditions of those two types of setups. In case of J-PET scanner the photons are gathered from much wider angle than in PALS. In PALS setup less of the photons that annihilate in source's protective layers reach the detector than in modular J-PET scanner. The differences in the components intensities between the measurements in same setup may come from differences in sources' casing (thickness and surface area of kapton and Parafilm foils) and, in case of PALS, from temperature fluctuation in the lab.

The intensities of components of the spectra from measurements with Quadra are not shown in this comparison as the ^{68}Ga source used in those measurements was applied in form of a solution. In case of this source the positrons do not have to pass through protective layers of kapton and parafilm, as it happens with sodium sources. The differences in constitution of ^{22}Na and ^{68}Ga sources result in incomparability of the intensities of fit parameters.

Table 6.8: The comparison of intensities of the fit parameters between spectra from measurements in PALS and modular J-PET. The main component intensity refers to the positron lifetime component in metals and ortho-positronium lifetime value in quartz glass. The additional component intensity relates to the sum of intensities of the rest of components of the spectra: the lifetime of positrons directly annihilating in kapton and Parafilm, para-positronium lifetime and ortho-positronium lifetime in Parafilm.

Sample disk	Main component intensity		Additional components intensity	
	PALS	J-PET	PALS	J-PET
Aluminum	81.00(11)	0.4384(15)	0.19	0.6992(24)
Copper	81.00(11)	0.5257(19)	0.19	0.6068(31)
Nickel	81.00(11)	0.5849(10)	0.19	0.42377(95)
Quartz	43.789(41)	0.52575(91)	0.5887(13)	0.52744(92)

6.4.5 Total number of counts

The uncertainty depends on the detector time resolution, the expected lifetime and number of counts in the spectra. The influence of the number of counts N (without the background) for the search of the component with given expected value of τ_E on the value of uncertainty s is given by equation:

$$s = \frac{\tau_E}{\sqrt{N}}, \quad (6.3)$$

If the statistics of the measurement are high enough, then the value of uncertainty is only impacted by the time resolution of the detector. In all of measurements presented in this thesis the number of collected counts for each spectra is high enough not to raise the uncertainty of the fitting.

In the Table 6.9 the total number of counts without the background is presented for measured data from PALS, modular J-PET and Biograph Vision Quadra.

Table 6.9: Number of counts forming the spectra for certain disks measured by PALS, modular J-PET and Biograph Vision Quadra. The presented numbers do not include the counts comprising the background. The number of counts presented for PALS measurements was collected on average for about 60 hours per each sample, the J-PET measurements spanned for 24 hours and measurements with Biograph Vision Quadra lasted for 1 hour. The activities of the sources used in those measurements varied, as described in section section 4.2.

Sample	Total # of counts		
	PALS [$\cdot 10^7$]	J-PET [$\cdot 10^5$]	Quadra [$\cdot 10^5$]
Aluminum	1.58104	5.72972	10.1855
Copper	1.58134	3.56672	3.94592
Nickel	1.68228	10.0808	6.91974
Quartz	1.57884	11.1451	5.76778

6.4.6 Width of the bins

It was shown that the measure of error of the fitted parameters from the theoretical values is dependent on the width of the bin of a distribution. The width of the bin of the data from PALS system is equal to 0.2 ns and for the Biograph Vision Quadra it is equal to 0.3 ns. The bin width of the distribution from modular J-PET is set to 0.5 ns. The simulations have shown around twice better accuracy of the fitting for in ranges 0.2 to 0.3 ns than 0.5 ns [14].

7. Summary and perspectives

The aim of this thesis was to compare the positronium time difference spectra obtained with three detectors: PALS, modular J-PET scanner and Biograph Vision Quadra scanner. It has been realised with disks of high purity materials: aluminum, copper, nickel and quartz glass. This study is the first comparative study of positronium imaging done with two types of PET detectors: modular J-PET and Biograph Vision Quadra scanners. The results of the analysis have confirmed the research hypothesis stated in this thesis, that the detection setups presented here are capable of positronium imaging. All three detection setups allow for good distinction between the positron lifetime in metals and ortho-positronium lifetime in quartz glass.

Within the framework of this thesis the author has performed multiple measurements using the PALS setup, modular J-PET scanner and took part in the measurements performed at the Inselspital in Bern with Biography Vision Quadra by Siemens. To correctly assess the values of spectra fitting parameters the author had, prior to the designated measurements, established the values of fit parameters for kapton and parafilm that enveloped the source that has been used in later studies with PALS and modular J-PET setups. The author had also preselected and analysed the data from the PALS and the modular J-PET measurements and analysed the data that were provided by the doctor William Steinberger after the measurements in Bern.

This work presents the basics of the positronium physics and the overview of the state of knowledge about positronium lifetime studies of biological material and its perspectives in medical diagnostics. It also shortly describes the characteristics of the positronium imaging systems. The thesis expands on the experimental setups and presents methods of data analysis for each of the detector.

It describes the signal analysis of the PALS measurements, the details of the data preselection with J-PET Framework software adapted for the purpose of lifetime spectra extraction by the author of this thesis and also briefly describes the conditions of data preselection for Biograph Vision Quadra spectra. The acquired lifetime difference spectra were analysed by the author with PALS Avalanche software.

Additionally, this thesis presents the methodology of the analysis of lifetime spectra for the sodium source encapsulated in protective layers of kapton and parafilm, which play an important role in interpretation of the lifetime spectra of researched samples.

In the last step of the analysis the values of significant components were established for the spectra from PALS, modular J-PET and Biograph Vision Quadra measurements. In case of metal disks of aluminum, copper and nickel, the main objective of the study was to compare the mean positron lifetimes that result from positron annihilation in metal lattice and its defects.

The comparison of the results has shown that for the aluminum disks the τ_{Al} values are consistent in 30% between the PALS and modular J-PET measurements and in 0.66% between PALS and Biograph Vision Quadra measurements. For the nickel disks the τ_{Ni} values are consistent in 31% between the PALS and modular J-PET measurements and in 2.6% between PALS and Biograph Vision Quadra measurements. For the copper disks the τ_{Cu} values are consistent in 5.6% of their value between the PALS and modular J-PET measurements and in 7% of their values between PALS and Biograph Vision Quadra measurements. Overall the positron mean lifetime values obtained with PALS and Biograph Vision Quadra convey the relation presented in literature, in which the positron lifetime in

bulk for nickel and copper were calculated as shorter than for aluminum [48]. The positron mean lifetime values obtained with modular J-PET do not exhibit this relation as the lifetime in copper was determined to be longer than in nickel and aluminum. It is worth to note though that the given samples may not convey the relation presented in literature due to the defects developed in the production process.

In case of quartz disks, the main searched component of the spectra was the ortho-positronium mean lifetime in quartz glass structure. For the quartz glass disks the τ_{o-Ps} values are consistent in 10% between the PALS and modular J-PET and 3.1% between PALS and Biograph Vision Quadra measurements. The ortho-positronium mean lifetime value for quartz glass is, as expected, one magnitude longer than mean positron lifetimes in metal disks and is in agreement with the literature value within two standard deviations for the results determined from PALS measurement and Biograph Vision Quadra measurement and within three standard deviations for the result of modular J-PET measurements [10].

There is an array of factors that may have impacted the precision of determining the lifetime values: the main factor being the timing resolution of the setups. It was also observed that the difference in samples placement inside the scanner during the measurement affects the time difference resolution of the spectra. The most precise mean lifetime values are obtained for the sample at the center of the detector. To improve the precision of the positronium mean lifetime determination it would be required to alter the measurements procedure to eliminate the differences in the measurement methodology. This study, due to the availability of resources, made use of ^{22}Na in measurements with PALS and modular J-PET scanner and ^{68}Ga source in measurement with Biograph Vision Quadra. Another aspect that could raise the precision of lifetime spectra analysis is to set the precise method of data selection and work at the analysis software in order to correct the estimation of intensities of the components of the fit. The modular J-PET scanner is not fully optimised yet, as it is in a prototype stage with the aim of developing the Total Body J-PET. The Total Body J-PET scanner, with an axial field of view of 2.5 meters, will allow for achievement of better timing resolution and efficiency of photons registration [74].

The results show that it is possible to discern between the samples characterised by different mean positron and positronium lifetime values, which may translate into development of the method of precision assessment for the positronium imaging setups. Especially important is the possibility of precise positronium lifetime value determination in ranges of nanoseconds, showcased with the quartz glass sample, as it represents the positronium lifetime characteristic for biological structures. As the biological materials undergo chemical and molecular changes, biological samples may not be reliable for purposes of calibration and quality assessment. The quartz glass material comprises the adequate reproduction of similar mean lifetime values. The results may serve to compose the quality assessment norm of positronium imaging detectors.

Bibliography

- [1] S. D. Bass et al. “Colloquium: Positronium physics and biomedical applications”. In: *Reviews of Modern Physics* 95.2 (2023), p. 021002.
- [2] P. Moskal et al. “Positronium in medicine and biology”. In: *Nature Reviews Physics* 1.9 (2019), pp. 527–529.
- [3] P. Moskal et al. “Positronium imaging with the novel multiphoton PET scanner”. In: *Science Advances* 7.42 (2021), eabh4394.
- [4] P. Moskal. “Positronium imaging”. In: *2019 IEEE nuclear science symposium and medical imaging conference (NSS/MIC)* (2020), pp. 1–3.
- [5] B. Jasińska et al. “Human Tissues Investigation Using PALS Technique”. In: *Acta Physica Polonica B* 48.10 (2017), p. 1737. ISSN: 1509-5770.
- [6] Y. Jean et al. “Applications of slow positrons to cancer research: Search for selectivity of positron annihilation to skin cancer”. In: *Applied surface science* 252.9 (2006), pp. 3166–3171.
- [7] G. Liu et al. “Further search for selectivity of positron annihilation in the skin and cancerous systems”. In: *Applied Surface Science* 255.1 (2008). Proceedings of the Eleventh International Workshop on Slow Positron Beam Techniques for Solids and Surfaces, pp. 115–118.
- [8] E. Kubicz. “Biomedical applications of Positron Annihilation Lifetime Spectroscopy: nanostructural characterization of normal and cancer cells and tissues”. PhD thesis. Jagiellonian University, 2021.
- [9] S. Niedźwiecki et al. “J-PET: a new technology for the whole-body PET imaging”. In: *Acta Physica Polonica B* 48 (2017), p. 1567.
- [10] W. Steinberger et al. “Positronium Lifetime Validation Measurements using a Long-Axial Field-of-View Positron Emission Tomography Scanner”. In: *EJNMMI physics* (2024).
- [11] P. Moskal et al. “Feasibility study of the positronium imaging with the J-PET tomograph”. In: *Physics in Medicine & Biology* 64.5 (2019), p. 055017.
- [12] P. Moskal et al. “Testing CPT symmetry in ortho-positronium decays with positronium annihilation tomography”. In: *Nature communications* 12.1 (2021), p. 5658.
- [13] P. Moskal et al. “Developing a novel positronium biomarker for cardiac myxoma imaging”. In: *EJNMMI physics* 10.1 (2023), p. 22.
- [14] K. Dulski. “Development of positronium imaging with the 192-strip J-PET detector”. PhD thesis. Jagiellonian University, 2022.
- [15] P. Moskal et al. “First positronium image of the human brain in vivo”. In: *Science Advances* (2024).

- [16] G. Łapkiewicz et al. “Developing a phantom for the positronium imaging evaluation”. In: *Acta Physica Polonica. B, Proceedings Supplement* 15.4 (2022).
- [17] G. Łapkiewicz. “Application of XAD4 water solutions for positronium imaging phantom”. Bachelor’s Thesis. Jagiellonian University, 2022.
- [18] P. Maheshwari et al. “Positron Probing of Liquid-free Volume To Investigate Adsorption–Desorption Behavior of Water in Two-Dimensional Mesoporous SBA-3”. In: *The Journal of Physical Chemistry C* 121.32 (2017), pp. 17251–17262.
- [19] P. G. Coleman. *Positron beams and their applications*. World Scientific, 2000.
- [20] B. Zgardzińska et al. “Studies on healthy and neoplastic tissues using positron annihilation lifetime spectroscopy and focused histopathological imaging”. In: *Scientific Reports* 10.1 (2020), p. 11890.
- [21] A. V. Avachat et al. “Positron annihilation lifetime spectroscopy of adipose, hepatic, and muscle tissues”. In: *Research Square* (2022).
- [22] S. Sharma et al. “Feasibility studies for imaging $e^+ e^-$ annihilation with modular multi-strip detectors”. In: *Nuclear Instruments and Methods in Physics Research Section A: Accelerators, Spectrometers, Detectors and Associated Equipment* 1062 (2024), p. 169192.
- [23] F. T. Ardebili. “Evaluation of the NEMA characteristics for the Modular J-PET scanner”. PhD thesis. Jagiellonian University, 2024.
- [24] URL: <https://www.siemens-healthineers.com/molecular-imaging/pet-ct/biograph-vision-quadra>.
- [25] G. A. Prenosil et al. “Performance characteristics of the Biograph Vision Quadra PET/CT system with a long axial field of view using the NEMA NU 2-2018 standard”. In: *Journal of nuclear medicine* 63.3 (2022), pp. 476–484.
- [26] K. Dulski et al. “Commissioning of the J-PET detector in view of the positron annihilation lifetime spectroscopy”. In: *Hyperfine Interactions* 239 (2018), pp. 1–6.
- [27] K. Dulski et al. “Analysis procedure of the positronium lifetime spectra for the J-PET detector”. In: *Acta Physica Polonica. A* 132.5 (2017), pp. 1637–1640.
- [28] M. Hasegawa et al. “Positron and positronium in free volume in oxides: silica glass and neutron-irradiated alumina”. In: *Materials Science Forum*. Vol. 175. Trans Tech Publ. 1994, pp. 269–278.
- [29] W. Steinberger et al. *Positronium Lifetime Measurements using Biograph Vision Quadra (Siemens Healthineers)*. 2023.
- [30] E. Kubicz et al. “Studies of unicellular microorganisms by means of positron annihilation lifetime spectroscopy”. In: *Nukleonika* 60.4 (2015), pp. 749–753.
- [31] J. Čížek. “Characterization of lattice defects in metallic materials by positron annihilation spectroscopy: A review”. In: *Journal of Materials Science & Technology* 34.4 (2018), pp. 577–598.
- [32] M. Deutsch. “Evidence for the formation of positronium in gases”. In: *Physical Review* 82.3 (1951), p. 455.
- [33] A. Ore and J. Powell. “Three-photon annihilation of an electron-positron pair”. In: *Physical Review* 75.11 (1949), p. 1696.

- [34] P. A. M. Dirac. "A theory of electrons and protons". In: *Proceedings of the Royal Society of London. Series A, Containing papers of a mathematical and physical character* 126.801 (1930), pp. 360–365.
- [35] A. Czarnecki et al. "Recent Results in Positronium Theory". In: *The Hydrogen Atom: Precision Physics of Simple Atomic Systems*. Ed. by S. G. Karshenboim et al. Berlin, Heidelberg: Springer Berlin Heidelberg, 2001, pp. 387–396.
- [36] S. Tao. "Positronium annihilation in molecular substances". In: *The Journal of Chemical Physics* 56.11 (1972), pp. 5499–5510.
- [37] S. Tao and J. Green. "Systematic positronium chemistry". In: *Journal of the Chemical Society A: Inorganic, Physical, Theoretical* (1968), pp. 408–417.
- [38] A. Mills Jr. "Positron and positronium sources". In: *Methods in Experimental Physics*. Vol. 29. Elsevier, 1995, pp. 39–68.
- [39] S. V. Stepanov and V. M. Byakov. "Electric field effect on positronium formation in liquids". In: *The Journal of chemical physics* 116.14 (2002), pp. 6178–6195.
- [40] M. D. Harpen. "Positronium: Review of symmetry, conserved quantities and decay for the radiological physicist". In: *Medical Physics* 31.1 (2004), pp. 57–61.
- [41] M. Eldrup et al. "The temperature dependence of positron lifetimes in solid pivalic acid". In: *Chemical Physics* 63.1 (1981), pp. 51–58.
- [42] B. Zgardzińska. "Can Tao-Eldrup Model Be Used at Short o-Ps Lifetime?" In: *Acta Physica Polonica A* 125.3 (2014), pp. 700–701.
- [43] Y. C. Jean. "Positron Annihilation in Polymers". In: *Positron Annihilation - ICPA-10*. Vol. 175. Materials Science Forum. Trans Tech Publications Ltd, Nov. 1994, pp. 59–70.
- [44] T. Goworek et al. "Positronium states in the pores of silica gel". In: *Chemical Physics* 230.2 (1998), pp. 305–315.
- [45] R. P. Gupta and R. Siegel. "Annihilation of a positron in a vacancy in aluminum". In: *Physical Review B* 22.10 (1980), p. 4572.
- [46] B. McKee et al. "Positron diffusion in metals and trapping at grain boundaries". In: *Philosophical Magazine A* 41.1 (1980), pp. 65–80.
- [47] R. Siegel. "Positron annihilation spectroscopy". In: *Annual Review of Materials Research* 10 (1980), pp. 393–425.
- [48] B. Barbiellini et al. "Calculation of positron lifetimes in bulk materials". In: *Journal of Physics: Condensed Matter* 3.39 (1991), p. 7631.
- [49] K. Hinode et al. "Positron lifetimes in deformed copper". In: *Journal of the Physical Society of Japan* 41.6 (1976), pp. 2037–2042.
- [50] T. Hehenkamp et al. "Positron lifetime spectroscopy in copper". In: *Journal of Physics F: Metal Physics* 16.8 (1986), p. 981.
- [51] A. Vertes et al. "Structure Studies of Nickel Electrodeposits: II. Positron Lifetime Measurements". In: *Journal of the Electrochemical Society* 131.7 (1984), p. 1526.
- [52] G. Dlubek et al. "Impurity-induced vacancy clustering in cold-worked nickel". In: *Journal of Physics F: Metal Physics* 9.10 (1979), p. 1961.
- [53] T. M. Hall et al. "Applications of positron-lifetime measurements to the study of defects in metals". In: *Physical Review B* 10.8 (1974), p. 3062.

- [54] D. W. Gidley, H.-G. Peng, and R. S. Vallery. “Positron annihilation as a method to characterize porous materials”. In: *Annu. Rev. Mater. Res.* 36.1 (2006), pp. 49–79.
- [55] R. A. Weinberg and R. A. Weinberg. *The biology of cancer*. WW Norton & Company, 2006.
- [56] J. D. Hayes et al. “Oxidative stress in cancer”. In: *Cancer cell* 38.2 (2020), pp. 167–197.
- [57] J. Pourahmad et al. “Role of oxygen free radicals in cancer development and treatment”. In: *Free radicals and diseases*. IntechOpen, 2016.
- [58] M. Assi. “The differential role of reactive oxygen species in early and late stages of cancer”. In: *American Journal of Physiology-Regulatory, Integrative and Comparative Physiology* 313.6 (2017), R646–R653.
- [59] M.-K. Zhang et al. “Tumor starvation induced spatiotemporal control over chemotherapy for synergistic therapy”. In: *Small* 14.50 (2018), p. 1803602.
- [60] B. Jasińska et al. “Human tissue investigations using PALS technique: free radicals influence”. In: *Acta Physica Polonica. A* 132.5 (2017), pp. 1556–1558.
- [61] K. Shibuya et al. “Oxygen sensing ability of positronium atom for tumor hypoxia imaging”. In: *Communications Physics* 3.1 (2020), p. 173.
- [62] P. Stepanov et al. “Interaction of positronium with dissolved oxygen in liquids”. In: *Physical Chemistry Chemical Physics* 22.9 (2020), pp. 5123–5131.
- [63] Y. Jean et al. “Applications of slow positrons to cancer research: Search for selectivity of positron annihilation to skin cancer”. In: *Applied Surface Science* 252.9 (2006). Proceedings of the Tenth International Workshop on Slow Positron Beam Techniques for Solids and Surfaces, pp. 3166–3171.
- [64] G. Liu et al. “Applications of positron annihilation to dermatology and skin cancer”. In: *physica status solidi c* 4.10 (2007), pp. 3912–3915.
- [65] E. Axpe et al. “Detection of atomic scale changes in the free volume void size of three-dimensional colorectal cancer cell culture using positron annihilation lifetime spectroscopy”. In: *PLoS One* 9.1 (2014), e83838.
- [66] A. Babińska. “Wyznaczenie parametrów czułości i swoistości testu dla czasu życia orto-Pozytonium w tkance nowotworowej raka jelita grubego”. Master’s thesis. Jagiellonian University, 2023.
- [67] S. Moyo et al. “Feasibility study of positronium application for blood clots structural characteristics”. In: *Bio-Algorithms and Med-Systems* 18.1 (2022).
- [68] J. Nizioł. “Development of experimental conditions for measuring the ortho-positronium lifetime in extracellular vesicles obtained in vitro”. Master’s thesis. Jagiellonian University, 2023.
- [69] T. Ahn et al. “Hierarchical nature of nanoscale porosity in bone revealed by positron annihilation lifetime spectroscopy”. In: *ACS nano* 15.3 (2021), pp. 4321–4334.
- [70] M. Chandrashekara and C. Ranganathaiah. “Chemical and photochemical degradation of human hair: A free-volume microprobe study”. In: *Journal of Photochemistry and Photobiology B: Biology* 101.3 (2010), pp. 286–294.
- [71] C. Wu et al. “PET imaging of inflammation biomarkers”. In: *Theranostics* 3.7 (2013), p. 448.

- [72] S. L. Kitson et al. “Clinical applications of positron emission tomography (PET) imaging in medicine: oncology, brain diseases and cardiology”. In: *Current Radiopharmaceuticals* 2.4 (2009), pp. 224–253.
- [73] J. C. Masdeu et al. “Imaging neuroinflammation in neurodegenerative disorders”. In: *Journal of nuclear medicine* 63.Supplement 1 (2022), 45S–52S.
- [74] P. Moskal and E. Stepień. “Prospects and clinical perspectives of total-body PET imaging using plastic scintillators”. In: *PET clinics* 15.4 (2020), pp. 439–452.
- [75] P. Moskal et al. “Test of a single module of the J-PET scanner based on plastic scintillators”. In: *Nuclear Instruments and Methods in Physics Research Section A: Accelerators, Spectrometers, Detectors and Associated Equipment* 764 (2014), pp. 317–321.
- [76] T. Matulewicz. “Radioactive nuclei for $\beta + \gamma$ PET and theranostics: selected candidates”. In: *Bio-Algorithms and Med-Systems* 17.4 (2021), pp. 235–239.
- [77] T. Bjørnstad et al. *Radiotracer generators for industrial applications, IAEA Radiation Technology Series No. 5*. Apr. 2013.
- [78] E. García-Toraño et al. “Standardisation and precise determination of the half-life of ^{44}Sc ”. In: *Applied Radiation and Isotopes* 109 (2016). Proceedings of the 20th International Conference on Radionuclide Metrology and its Applications 8–11 June 2015, Vienna, Austria, pp. 314–318.
- [79] J. E. Turner. *Atoms, radiation, and radiation protection*. John Wiley & Sons, 2008.
- [80] URL: <https://ehs.umich.edu/wp-content/uploads/2016/04/Sodium-22.pdf>.
- [81] S. R. Cherry et al. *PET: physics, instrumentation, and scanners*. Springer, 2006.
- [82] *Scionix*. URL: <https://scionix.nl/scintillation-crystals/#tab-id-4>.
- [83] *Eljen Technology*. URL: <https://eljentechnology.com/>.
- [84] S. Gundacker et al. “Vacuum ultraviolet silicon photomultipliers applied to BaF₂ cross-luminescence detection for high-rate ultrafast timing applications”. In: *Physics in Medicine & Biology* 66.11 (2021), p. 114002.
- [85] S. Gundacker et al. “Precise rise and decay time measurements of inorganic scintillators by means of X-ray and 511 keV excitation”. In: *Nuclear Instruments and Methods in Physics Research Section A: Accelerators, Spectrometers, Detectors and Associated Equipment* 891 (2018), pp. 42–52.
- [86] URL: https://www.advatech-uk.co.uk/lso_ce.html.
- [87] URL: <https://hub.hamamatsu.com/us/en/technical-notes/mppc-sipms/what-is-an-SiPM-and-how-does-it-work.html>.
- [88] *ISOMED 2010 Dose Calibrator*. URL: <https://www.nuviatech-healthcare.com/product/dose-calibrator/>.
- [89] W. Steinberger. personal communication. 2023.
- [90] K. Dulski. “Assembly and calibration of apparatus for Positron Annihilation Lifetime Spectroscopy”. Master’s thesis. Jagiellonian University, 2016.
- [91] K. Dulski. “PALS avalanche: a new PAL spectra analysis software”. In: *Acta Physica Polonica. A* 137.2 (2020).
- [92] G. Korcyl et al. “Evaluation of single-chip, real-time tomographic data processing on FPGA SoC devices”. In: *IEEE transactions on medical imaging* 37.11 (2018), pp. 2526–2535.

- [93] W. Krzemien et al. “J-PET Framework: Software platform for PET tomography data reconstruction and analysis”. In: *SoftwareX* 11 (2020), p. 100487.
- [94] W. Krzemień et al. “Analysis framework for the J-PET scanner”. In: *Acta Physica Polonica. A* 127.5 (2015), pp. 1491–1494.
- [95] *Parafilm*. URL: <https://www.amcor.com/products/technical-applications/sealing-films-wraps>.
- [96] B. Zgardzińska. “Ortho-positronium in liquid alkanes”. In: *Nukleonika* 55.1 (2010), pp. 41–46.

8. Appendix A - fitted spectra

8.1 PALS measurements spectra

The PALS Avalanche program allows for modifying a fitting configuration file, in which, additionally to setting the initial values of the fit components, the user can set the parameters listed below:

- arrangement of data (e.g. histogram or list of time differences),
- the width of the bins,
- minimal counts for the first and last bin (this parameter impacts background evaluation),
- how many bins will be used for background estimation,
- if the background will be estimated from the left or right side of the histogram,
- end of fit range,
- fixing or freeing the resolution component σ ,
- for how many σ the background can vary,
- the initial values of lifetimes and intensities (this is the starting value fitted to the spectra in the first iteration),
- number of iterations,
- component type

Explanation of names describing components in the Appendix can be found in section 5.2.

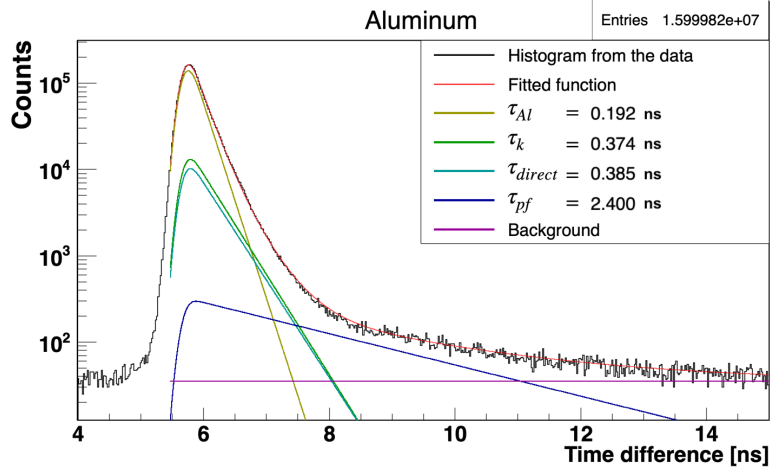


Figure 8.1: Fitted spectrum of merged data from all 4 aluminum measurements. The red line indicates the fitted function, the yellow line corresponds to the of the component with the positron mean lifetime of positron direct annihilation in aluminium disk τ_{Al} , while the green line - of the direct annihilation of positrons in kapton τ_k , the blue line - the direct annihilation in parafilm τ_{direct} , the dark blue line - the ortho-positronium annihilation in Parafilm. The purple line marks the background level that is calculated here as a mean value of 50 bins on the left side of the spectrum.

Table 8.1: Results of the fit for spectrum of all four aluminum disk measurements data sets merged together. The χ^2/dof value for this fit is 2.64. Fitted parameter of detector resolution $\sigma = 0.10395(11)$

Type	Lifetime [ns]	Intensity
τ_k	0.374	0.1
τ_{direct}	0.385	0.08
τ_{Al}	0.19207(16)	0.8100(11)
τ_{pf}	2.4	0.01

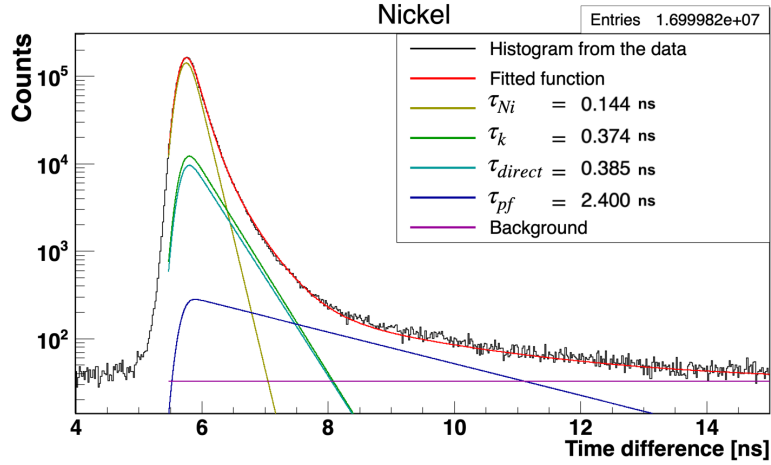


Figure 8.2: Fitted spectrum of merged data for all nickel measurements. The red line indicates the fitted function, the yellow line corresponds to the of the component with the positron mean lifetime of positron direct annihilation in nickel disk τ_{Ni} , while the green line - of the direct annihilation of positrons in kapton τ_k , the blue line - the direct annihilation in parafilm τ_{direct} , the dark blue line - the ortho-positronium annihilation in Parafilm. The purple line marks the background level that is calculated here as a mean value of 50 bins on the left side of the spectrum.

Table 8.2: Results of the fit for spectrum of all four nickel disk measurements data sets merged together. The χ^2/dof value for this fit is 2.09. Fitted parameter of detector resolution $\sigma = 0.10868(11)$

Type	Lifetime [ns]	Intensity
τ_k	0.374	0.1
τ_{direct}	0.38	0.08
τ_{Ni}	0.14388(14)	0.8100(11)
τ_{pf}	2.4	0.01

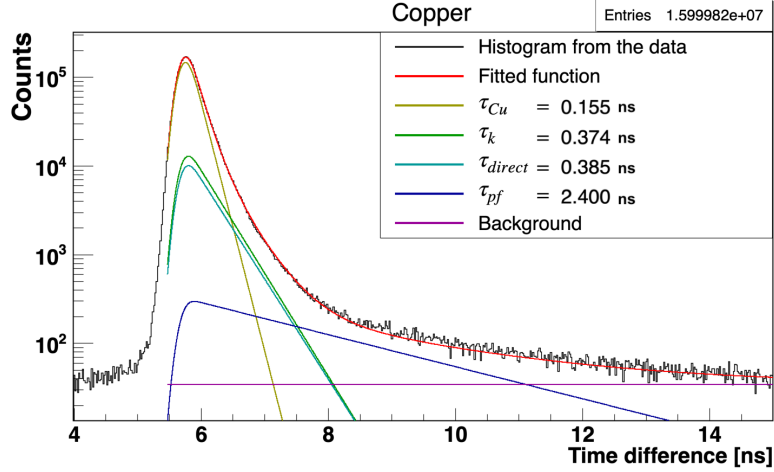


Figure 8.3: Fitted spectrum of merged data for all copper measurements. The red line indicates the fitted function, the yellow line corresponds to the of the component with the positron mean lifetime of positron direct annihilation in copper disk τ_{Cu} , while the green line - of the direct annihilation of positrons in kapton τ_k , the blue line - the direct annihilation in parafilm τ_{direct} , the dark blue line - the ortho-positronium annihilation in Parafilm. The purple line marks the background level that is calculated here as a mean value of 50 bins on the left side of the spectrum.

Table 8.3: Results of the fit for spectrum of all four copper disk measurements data sets merged together. The χ^2/dof value for this fit is 2.12. Fitted parameter of detector resolution $\sigma = 0.10783(11)$

Type	Lifetime [ns]	Intensity
τ_k	0.374	0.1
τ_{direct}	0.38	0.08
τ_{Cu}	0.15473(14)	0.8100(11)
τ_{pf}	2.4	0.01

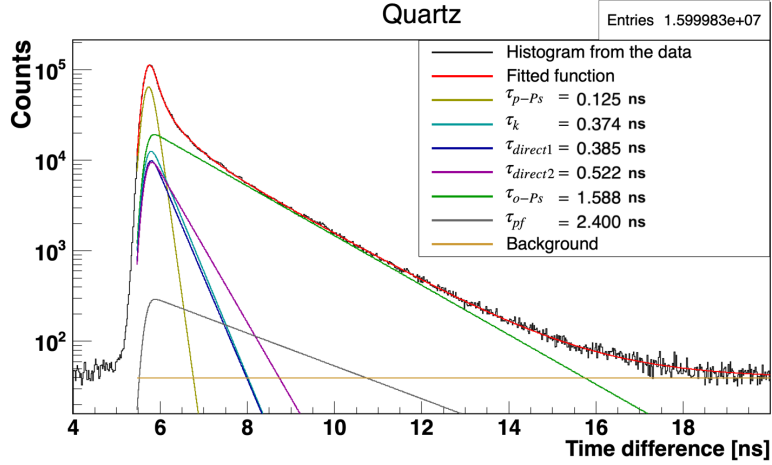


Figure 8.4: Fitted spectrum of merged data for all quartz measurements. The red line indicates the fitted function, the yellow line corresponds to the of the component with the para-positronium mean lifetime τ_{p-Ps} , while the blue line - the direct annihilation of positrons in kapton τ_k , the dark blue line - the direct annihilation in parafilm $\tau_{direct1}$, the purple line - the direct annihilation in quartz glass $\tau_{direct2}$, the green line - ortho positronium annihilation in quartz glass τ_{o-Ps} , the grey line - the ortho-positronium annihilation in parafilm. The orange line marks the background level that is calculated here as a mean value of 50 bins on the left side of the spectrum.

Table 8.4: Results of the fit for spectrum of all four quartz disk measurements data sets merged together. The χ^2/dof value for this fit is 1.98. Fitted parameter of detector resolution $\sigma = 0.11191(15)$

Type	Lifetime [ns]	Intensity
τ_{p-Ps}	0.125	0.30454(39)
τ_k	0.374	0.1
$\tau_{direct1}$	0.385	0.08
$\tau_{direct2}$	0.522(61)	0.09411(47)
τ_{o-Ps}	1.5877(15)	0.45799(43)
τ_{pf}	2.4	0.01

8.2 J-PET measurements spectra

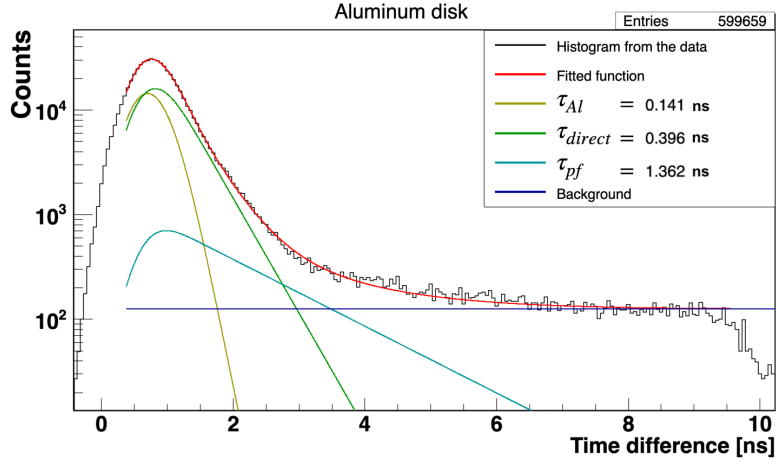


Figure 8.5: Fitted spectrum obtained for aluminum disk by modular J-PET. The red line indicates the fitted function, the yellow line corresponds to the of the component with the positron mean lifetime in aluminum τ_{Al} , the green line - the positron direct annihilation τ_{direct} , the blue line - the ortho-positronium annihilation in parafilm τ_{pf} . The purple line indicates the background level.

Table 8.5: Results of the fit of the spectra for aluminum disks form measurements with J-PET detector. The goodness of the fit measured as $\chi^2/dof = 15.16$. Fitted value of detector time resolution $\sigma = 0.27776(74)$

Type	Lifetime [ns]	Intensity
τ_{Al}	0.1414(15)	0.4384(15)
τ_{direct}	0.3959(11)	0.6421(15)
τ_{pf}	1.362(20)	0.05709(87)

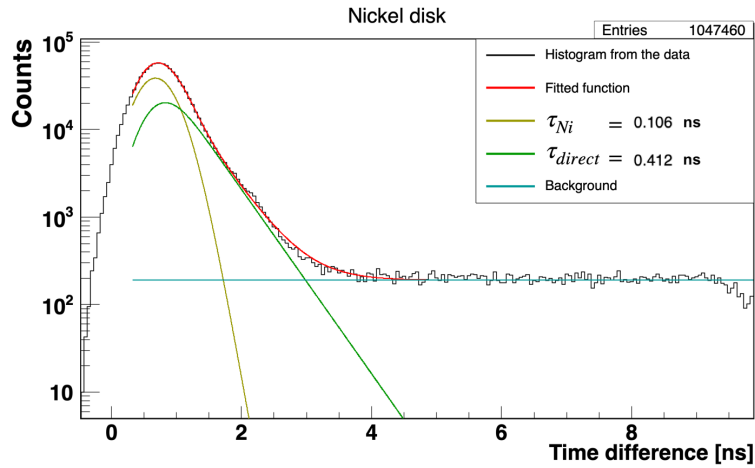


Figure 8.6: Fitted spectrum obtained for nickel disk by modular J-PET. The red line indicates the fitted function, the yellow line corresponds to the of the component with the positron mean lifetime in nickel τ_{Ni} , the green line - the positron direct annihilation τ_{direct} . The blue line indicates the background level.

Table 8.6: Results of the fit of the spectra for nickel disk form measurements with J-PET detector. The goodness of the fit measured as $\chi^2/dof = 5.18$. Fitted value of detector time resolution $\sigma = 0.28332(48)$

Type	Lifetime [ns]	Intensity
τ_{Ni}	0.10570(47)	0.5849(10)
τ_{direct}	0.41232(94)	0.42377(95)

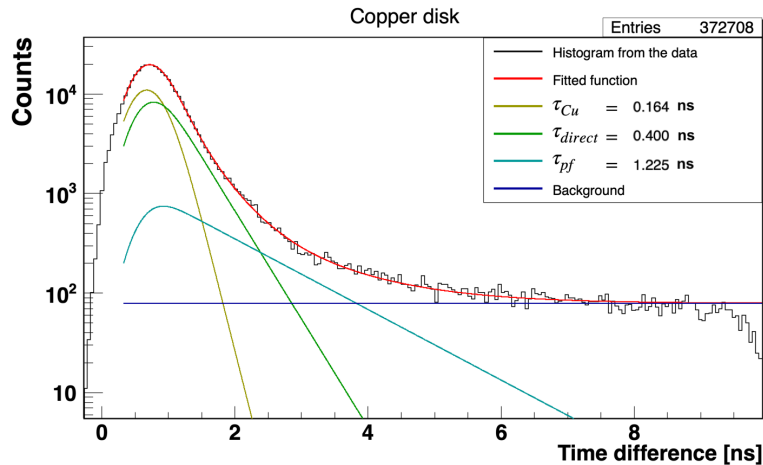


Figure 8.7: Fitted spectrum obtained for copper disk by modular J-PET. The red line indicates the fitted function, the yellow line corresponds to the of the component with the positron mean lifetime in copper τ_{Cu} , the green line - the positron direct annihilation τ_{direct} , the blue line - the ortho-positronium annihilation in parafilm τ_{pf} . The purple line indicates the background level.

Table 8.7: Results of the fit of the spectra for copper disks form measurements with J-PET detector. The goodness of the fit measured as $\chi^2/dof = 4.64$. Fitted value of detector time resolution $\sigma = 0.26857(91)$

Type	Lifetime [ns]	Intensity
τ_{Cu}	0.1637(14)	0.5257(19)
τ_{direct}	0.3999(17)	0.5189(19)
τ_{pf}	1.225(16)	0.0879(12)

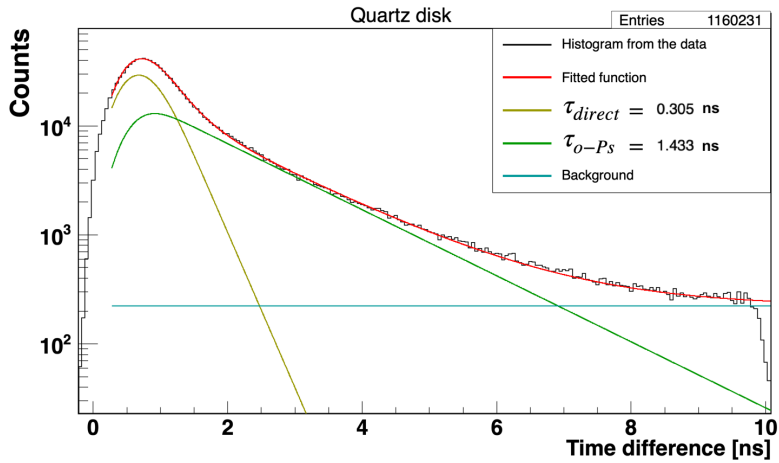


Figure 8.8: Fitted spectrum obtained for quartz disk by modular J-PET. The red line indicates the fitted function, the yellow line corresponds to the of the component with the positron mean lifetime τ_{direct} , the green line - the ortho-positronium annihilation in quartz glass τ_{o-Ps} . The blue line indicates the background level.

Table 8.8: Results of the fit of the spectra for quartz disk form measurements with J-PET detector. The goodness of the fit measured as $\chi^2/dof = 11.68$. Fitted value of detector time resolution $\sigma = 0.31755(72)$

Type	Lifetime [ns]	Intensity
τ_{direct}	0.3053(10)	0.52744(92)
τ_{o-Ps}	1.4331(27)	0.52575(91)

8.3 Biograph Vision Quadra measurements spectra

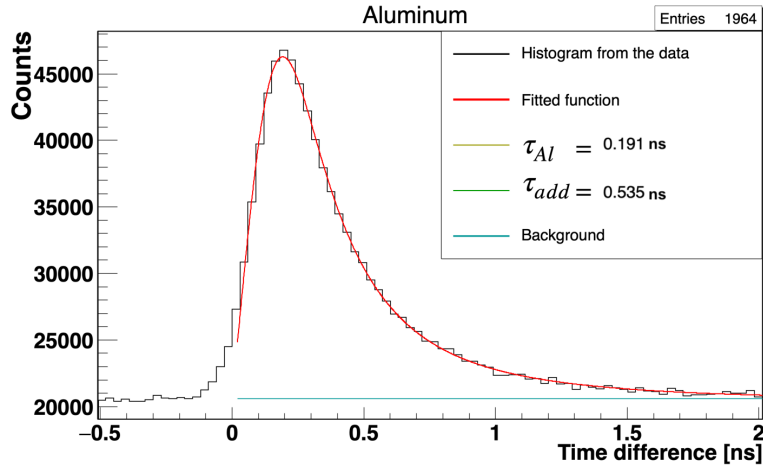


Figure 8.9: Fitted spectrum of data from the measurements in Biograph Vision Quadra for the aluminum disks. Value of χ^2/dof of this fit is 1.30. The value of sigma of this fit is 0.10541(55).

Table 8.9: Results of the fit for aluminum disks measured with Biograph Vision Quadra. χ^2/dof value for this fit is 1.30. The value of sigma of this fit is 0.10541(55).

Type	Lifetime [ns]	Intensity
τ_{Al}	0.1908(12)	05973(22)
τ_{add}	0.535	0.43

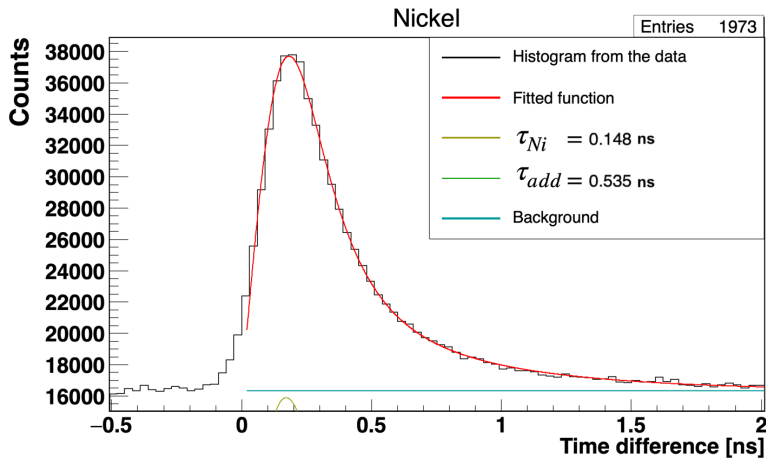


Figure 8.10: Fitted spectrum of data from the measurements in Biograph Vision Quadra for the nickel disks. Value of χ^2/dof of this fit is 1.26. The value of sigma of this fit is 0.10541(55).

Table 8.10: Results of the fit for nickel disks measured with Biograph Vision Quadra. χ^2/dof value for this fit is 1.26. The value of sigma of this fit is 0.10541(55).

Type	Lifetime [ns]	Intensity
τ_{Ni}	0.1477(11)	0.5222(22)
τ_{add}	0.535	0.43

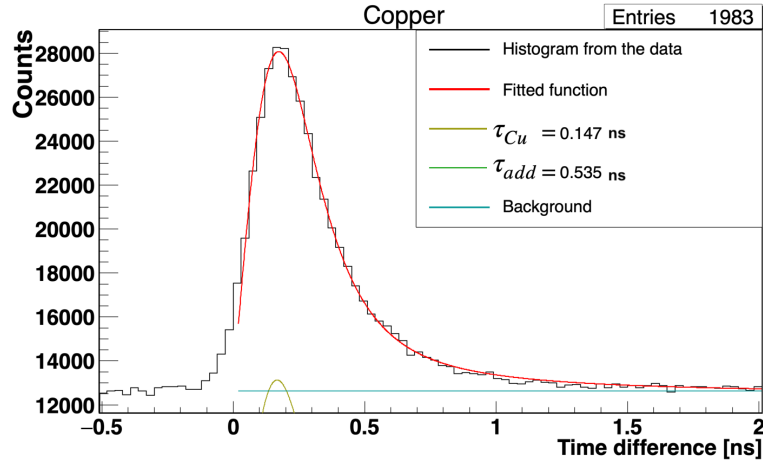


Figure 8.11: Fitted spectrum of data from the measurements in Biograph Vision Quadra for the copper disks. Value of χ^2/dof of this fit is 1.12. The value of sigma for this fit is 0.10227(65).

Table 8.11: Results of the fit for copper disks measured with Biograph Vision Quadra. χ^2/dof value for this fit is 1.12. The value of sigma for this fit is 0.10227(65).

Type	Lifetime [ns]	Intensity
τ_{Cu}	0.1659(12)	0.7517(32)
τ_{add}	0.535	0.2195(44)

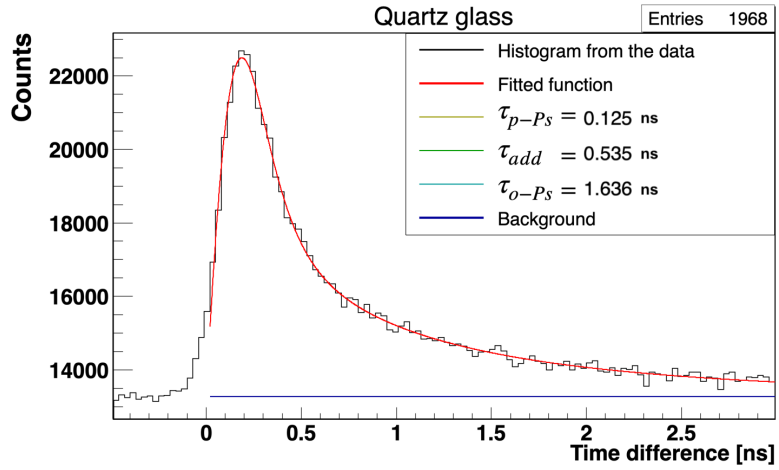


Figure 8.12: Fitted spectrum of data from the measurements in Biograph Vision Quadra for the quartz disks. Value of χ^2/dof of this fit is 0.97. Sigma value of this fit is 0.1261(12).

Table 8.12: Results of the fit for quartz disks measured with Biograph Vision Quadra. χ^2/dof value for this fit is 0.97. Sigma value of this fit is 0.1261(12).

Type	Lifetime [ns]	Intensity
τ_{p-Ps}	0.125	0.4148(41)
τ_{add}	0.535	0.43
τ_{o-Ps}	1.636(28)	0.863(10)